Progress in Particle and Nuclear Physics 125 (2022) 103964

Contents lists available at ScienceDirect

Progress in Particle and Nuclear Physics

journal homepage: www.elsevier.com/locate/ppnp

Review

Antiprotonic bound systems

M. Doser

CERN, Switzerland

ARTICLE INFO

Article history:
Available online 21 April 2022

Keywords:
Antiprotonic atoms
Antihydrogen
Protonium
HCI
Radioisotope
Antiprotonic ions

ABSTRACT

A wide range of exotic bound systems incorporating antiprotons (atoms, atomic ions, molecules or molecular ions) can be formed, in many cases simply by replacing at least one electron of a matter system by an antiproton. A number of these systems have been studied over decades, while others (in particular antihydrogen) have only recently been the object of precision measurements, and a much larger set have not yet been explored. This review focuses on the physics topics that these exotic systems allow to investigate, and that range from tests of fundamental symmetries to investigating the strong and electromagnetic interactions to probing nuclear models in nuclei far from the line of stability.

Contents

E-mail address: michael.doser@cern.ch.

https://doi.org/10.1016/j.ppnp.2022.103964

1. Introduction

The study of antiprotons and, of specific interest to this review, of exotic atoms containing antiprotons (antihydrogen, antiprotonic helium, protonium, but also other atoms, ions or molecules in which an electron is replaced by an antiproton) provides many windows into the investigation of fundamental symmetries, of interactions between particles and nuclei, of nuclear physics and of atomic physics. This field appeared simultaneously with the first accelerators, and has advanced over the decades in parallel with improvements and advances in its infrastructure, mainly at CERN, but also at KEK, BNL and others.

The symmetries amenable to investigation by these systems are CPT (investigated via precision spectroscopy of antihydrogen or antiprotonic atoms) and the weak equivalence principle through measurements of the gravitational interaction of (neutral) antiprotonic atoms (antihydrogen, but other neutral antiprotonic systems are also suitable). Further precision tests are also possible: tests of QED in antiprotonic Rydberg atoms [1], searches for anomalous terms in the strong interaction [2], investigation of nuclei and nuclear models [3], and more generally, searches for "beyond standard model" (BSM) physics (specifically, in the framework of the Standard Model Extension [4,5] or e.g. in searches for a putative $\bar{p}$EDM). The simplest antiprotonic bound system is protonium, a bound state of an antiproton with a proton, which was formed by slowing down antiprotons (by ionization loss) in hydrogen, but even the simplest system formed completely of antimatter, antihydrogen, already required substantially more advanced efforts. Of course, antiprotonic atoms with heavier nuclei, as well as complex systems, including antiprotonic molecules or molecular ions, are also possible.

The study of these exotic systems does not quite follow the general history of particle physics: while accelerators at CERN became ever more powerful over the decades, the energies required to produce antiprotons are modest; even today, the same Proton Synchrotron (PS) that produced the first antiprotons at CERN in 1960 [6], shortly after its start-up in 1959 still continues to provide the antiprotons that form the heart of experiments on them or on atoms containing them. Nevertheless, technical developments at CERN have played a defining role in the study of antiprotonic systems. In particular, experiments relying on background-free beams of antiprotons have only become possible through the invention of stochastic cooling, the construction of a dedicated storing and cooling accelerator infrastructure (the Antiproton Accumulator (AA) and the Antiproton Collector (AC)), and the development of antiproton trapping techniques in the 1980's at CERN's dedicated antiproton experimental facility LEAR (low energy antiproton ring) from 1982 to 1996. Since 2000, the AC, transformed into the unique Antiproton Decelerator (AD) facility, hosts all existing experiments worldwide that require trapped antiprotons. Commissioned in 2018, a further deceleration stage in form of the ELENA decelerator [7] will increase the number of trappable antiprotons 100-fold.

Instead of following a historical path, and in light of the existence of a number of excellent earlier and recent reviews of antiprotonic atoms ([8–14] among others), this review will instead focus on substantial advances (mainly in antihydrogen and antiprotonic helium) or re-evaluations that occurred in the last decade and structure these in terms of individual antiprotonic bound systems of increasing complexity, starting with antihydrogen, then protonium, then antiprotonic atoms (as well as antiprotonic ions) with stable nuclei. The later sections will then deal with longer term possibilities, among them antiprotonic atoms with stable or unstable nuclei, antiprotonic molecules, and finally, antiprotonic molecular ions, and point out the specific physics questions that a study of these systems can allow to shed light on. Hadronic effects are only briefly touched upon, given that little new data are available, although this situation may change again in the future. Other topics (from tests of fundamental symmetries to nuclear physics) are however addressed in more detail, as future developments will likely have wide bearing on these. Table 1 gives an overview of the different systems that will be covered in this review, and indicates which formation processes (which will be discussed in the following), physics thrust and experimental methodology are relevant for each of them.

Table 1
Overview of the main systems covered in this review.

System	Section	Formation process	Physics subjects	Experimental techniques
$\bar{H}$	2	3-body recombination, charge exchange with Ps	CPT, WEP, BSM, $\rho(\bar{p})$	laser and microwave spectroscopy, free fall
$\bar{p}$p, $\bar{p}$d	3	atomic capture, pulsed charge exchange	strong interaction, CPT	fluorescence & laser spectroscopy
$\bar{p}$He	4	atomic capture	strong interaction, CPT, QED	fluorescence & laser spectroscopy
antiprotonic atoms $\bar{p}$A (Z >2)	5	pulsed charge exchange with Rydberg atoms, $\bar{p}$ + A^+	strong interaction, nuclear physics, QED, BSM, CPT	spectroscopy (laser, fluorescence, meson), mass spectrometry
$\bar{p}$ ionic systems ($\bar{H}^-$, $\bar{p}A^{++}$, hollow $\bar{p}$-HCI's)	6	double charge exchange, $\bar{p}$ + A^+, $A^{Z+} + \bar{p}p^*$	QED, BSM	laser spectroscopy
antiprotonic molecules ($\bar{H}_2$, $\bar{H}_2^+$, ...) & molecular ions	7	$\bar{H} + \bar{H}$, pulsed charge exchange, laser-assisted formation	CPT	laser spectroscopy

1.1. Formation of antiprotonic systems

Formation of antiprotonic systems has, before the advent of the AD, relied on injecting antiprotons into bulk matter (solid, liquid or gaseous). In these bulk systems, antiprotons lose energy via collisions with electrons until their energy matches the binding energy of the electrons of the target material, one of which it will replace, leading to the formation of an excited antiprotonic system. In the case of a hydrogen target for example, Rydberg protonium is formed in a broad range of n,l states [15,16].

The same process also occurs for other target nuclei, with the additional complication of Auger emission of the target nucleus' electrons, and with the noteworthy exception of antiprotonic helium, the full cascade, possibly expedited by Stark mixing (for Z=1 and 2), collisional de-excitation or quenching, is over in $\sim 10^{-9}$ s, at which point annihilation of the antiproton with a neutron or a proton at the periphery of the nucleus takes place.

With the advent of the possibility of trapping antiprotons, production processes allowing much greater control, in particular formation of antiprotonic systems in Penning traps, became feasible: antihydrogen formation in traps was proposed already in 1986 [17]. Several antihydrogen production processes that interact antiprotons ($\bar{p}$) with positrons (e^+) or positronium (Ps) have been envisaged:

$$\bar{p} + e^+ + e^+ \rightarrow \bar{H} + e^+ \quad (1)$$

$$\bar{p} + Ps \rightarrow \bar{H} + e^- \quad (2)$$

$$\bar{p} + e^+ + n\gamma \rightarrow \bar{H} + (n+1)\gamma \quad (n \geq 0) \quad (3)$$

Similarly, mixing processes of trapped antiprotons with positively charged ions, intentionally or through the presence of positively charged (atomic or molecular) ions or of neutral atoms, can lead to formation of e.g. protonium [18] or of antiprotonic atoms under conditions that exclude interactions with other atoms that might perturb the subsequent evolution of the bound system.

Cross sections for charge exchange reactions leading to antiprotonic atoms (protonium, antiprotonic helium) or antihydrogen have been calculated both via classical-trajectory Monte Carlo simulations or explicitly. The resulting cross sections are strongly dependent on the relative energies between the antiproton and the atomic system, as well as on the inner state of that atom: cross sections for protonium formation through interactions between antiprotons and ground state hydrogen atoms lie in the range of $10^{-16} \sim 10^{-14}$ cm^{-2} for relative energies between 10 eV and 10 meV [19–21] and similar values pertain for the formation of antiprotonic atoms through antiproton–atom interactions (e.g. antiproton–neon interactions, Fig. 1, left). A comparable cross section of 10^{-15} cm^{-2} for the formation of antihydrogen is obtained for the charge exchange process (2) with ground state positronium, which however increases with n^4 for positronium in Rydberg states with principal quantum number n [22] and can thus reach values approaching or even exceeding 10^{-8} cm^{-2} under realistic experimental conditions (Fig. 1, right).

The situation is different for the three-body process (1): here, a quadratic dependence on the positron density and a $T^{-9/2}$ temperature dependence imply the need for cold, dense positron plasmas [23], for which however production rates of 10^3 $\bar{H}$/s can be reached with O(10^5) antiprotons interacting with O(10^6) positrons. Of more interest (in view of trapping) is the energy distribution of the resulting antihydrogen atoms (Section 2.2.1). Similar production rates for antiprotonic atoms and molecules should be expected when starting with antiprotons and a cationic plasma, although a low relative velocity between antiprotons and cations for the same plasma temperature should lead to significant enhancements [24]. Section 5.2 discusses these systems and their formation rates in more detail.

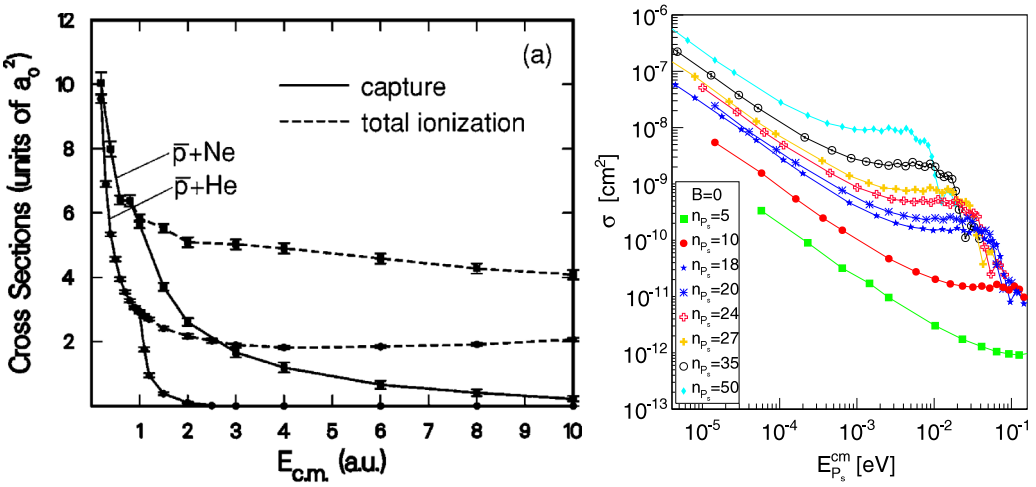

Fig. 1. Left: (a) Formation cross section ($a_0^2 = 0.28 \times 10^{-16}$ cm^2) for the antiprotonic atoms $\bar{p}$-He and $\bar{p}$-Ne [25]. Right: Formation cross section for antihydrogen via the charge exchange process (2) for different values of the positronium principal quantum number n_{Ps} [22]. Reproduced with permission.

2. Antihydrogen atoms

The above controlled antihydrogen formation processes however require large numbers of positrons (three-body formation, (1)), production and transport of positronium towards trapped antiprotons (charge exchange, (2)), or have a very low cross section (radiative formation, (3)). In 1994, before the positron accumulation technique based on radio-isotope decays developed in 1989 by the group of C. Surko [26] had become advanced enough that the required numbers of positrons were routinely available for antihydrogen production in Penning traps to be attempted, an alternative route was proposed by members of the PS202 experiment [27] to produce antihydrogen atoms in flight, using the interaction between the antiprotons stored in the LEAR ring and a jet-gas target consisting of Xe atoms. The production process of antihydrogen is then:

$$\bar{p}Z \rightarrow \bar{H}e^{-}Z \tag{4}$$

where the requisite positron–electron pairs are formed via the space-like interaction between photons formed by the antiprotons in the Coulomb field of the nucleus with charge Z, allowing the $\bar{p}$ to capture the co-moving positron and form antihydrogen. The experiment (called PS210) was carried out during 15 h in the course of 1995. With an integrated luminosity (based on the number of antiprotons and the gas-target thickness) of $\mathcal{L} = 5 \times 10^{33}$ cm^{-2}, a total of 11 antihydrogen atom candidate events [28] were detected (with an estimated background of 2 events). Although the high momentum of the antiproton beam (1.94 GeV/c) meant that the resulting antihydrogen atoms could not be studied, this proof-of-principle experiment, together with a similar experiment at Fermilab [29], gave great support to the subsequent modification of the AC into a full-fledged antiproton deceleration facility at which antihydrogen production in Penning traps, trapping of the produced antihydrogen atoms, and precision spectroscopy of these atoms could be attempted.

2.1. Low energy antihydrogen

Several proposals to carry out experiments at this new antiproton facility, the Antiproton Decelerator, planned for 1999, were submitted as soon as its construction had been decided. Both ATHENA (AD-1) and ATRAP (AD-2) were based on a similar experimental design: a multi-well Penning trap (in a so-called "nested well" potential configuration, Fig. 2) that would hold antiprotons and positrons simultaneously in neighboring, opposite polarity Penning trap wells, and allow bringing them into contact in a controlled manner. In both experiments, the produced antihydrogen atoms – being neutral – would leave the formation region.

The first observation (Fig. 2, left) of the production of antihydrogen via mixing of antiprotons and positrons (three-body recombination) was provided by ATHENA [30], followed only a few weeks later by a confirmation of the process by ATRAP [31] (Fig. 2, right). Detection of antihydrogen formation in the ATHENA case was via reconstruction of the annihilation vertex of the antiproton on the Penning trap inner surface (reconstructed through a two-layer double-sided silicon micro-strip detector that detected the annihilation pion trajectories) and of the opening angle (with respect to the reconstructed annihilation vertex) of the two (simultaneously detected) 511 keV photons produced in the positron annihilation: an excess of back-to-back emission was the signal for antihydrogen annihilation. In the case of the ATRAP experiment, detection of $\bar{H}$ was performed by field-ionizing the produced atoms, and subsequently detecting the

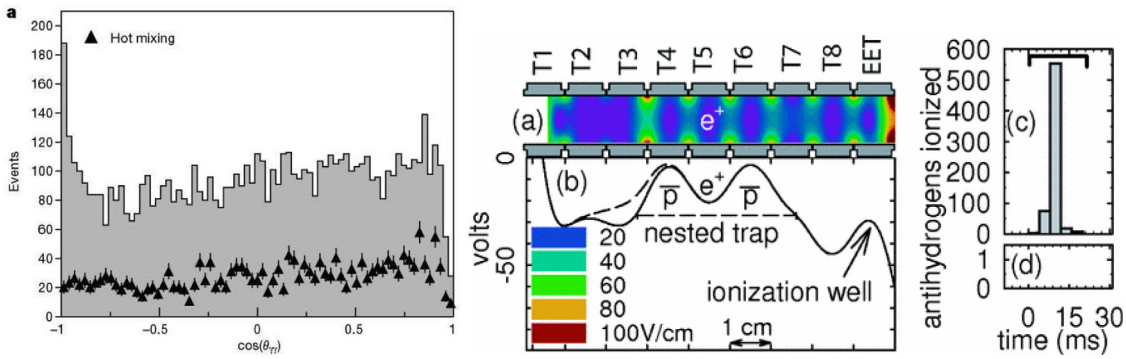

Fig. 2. Left: ATHENA experiment: Angular distribution between two detected photons from e^+e^- annihilation as reconstructed from the simultaneously detected antiproton annihilation vertex. The peak at $cos(\theta) = -1$, but also the bulk of the distribution, corresponds to antihydrogen annihilations. The 'hot mixing' data correspond to mixing of cold antiprotons with RF-heated positrons, where no antihydrogen production can take place [30]; Right: (a) Electrodes for the ATRAP nested Penning trap, upon which a representation of the magnitude of the electric field that strips $\bar{H}$ atoms is superimposed. (b) Potential on axis for positron cooling of antiprotons (solid line) during which $\bar{H}$ formation takes place, with the (dashed line) modification used to launch $\bar{p}$ into the well. (c) Antiprotons from $\bar{H}$ ionization are released from the ionization well during a 20 ms time window. (d) No $\bar{p}$ are counted when no e^+ are in the nested Penning trap [31]. Reproduced with permission.

resulting, trapped, antiprotons, a scheme well matched to the 3-body production process employed also in their case, and which produces mostly highly excited states of antihydrogen. This observation furthermore yielded information on the production process, since field-ionization of antihydrogen would not have allowed detecting deeply bound antihydrogen atoms, such as would have been produced in the competing radiative production process of Eq. (3).

Further information on the distribution of populated antihydrogen states could also be immediately obtained via the same field-ionization detection scheme by varying the ionizing field strength [32]. This confirmed that antihydrogen formed by mixing antiprotons and positrons in a nested-well Penning trap is mainly produced in Rydberg states and that these atoms are relatively hot (Fig. 4, right). Subsequent analyses of plasma physics processes and simulations of the interaction of Rydberg antihydrogen atoms with the dense positron plasma confirmed and finessed this picture [33]. The formation process involved in (1) requires comparable velocities between antiprotons and positrons; it is thus the temperature of the positron plasma that determines the velocity (and thus the equivalent 'temperature') of the formed antihydrogen atoms.

The same scheme of mixing antiprotons with trapped positrons in a nested trap configuration is also employed by the ASACUSA collaboration, albeit in a trap sited in an axially non-homogeneous magnetic field ("cusp trap" [34]). Injection of low energy ($\sim$ eV) antiprotons from an intermediate trap into a nested well configuration (rapidly-switched from the injection configuration) allows interacting $3 \times 10^5 \bar{p}$ with $3 \times 10^7 e^+$ over timescales of 10's of seconds. Field ionization of any formed Rydberg antihydrogen atoms allows determining the flux in direction of the downstream coil, which forms the second oppositely polarized part of the anti-Helmholtz configuration that preferentially selects low-field seeking antihydrogen states. The resulting flux of several $\bar{H}$ atoms per second [35] (Fig. 3, right) decreases over time as the positron and antiproton plasmas axially separate in the nested trap configuration through collisional relaxation (with the positrons) or sympathetic cooling (with co-trapped electrons). This decrease in $\bar{p}$ axial energy can be counteracted by applying an rf drive on the electrodes of the nested trap well. The question of whether this approach leads to preferentially emitted, deeply bound $\bar{H}$ atoms as are needed for the measurement of the ground state hyperfine splitting that is the goal of this setup will be discussed in 2.2.2.

An alternative to the nested well technique of producing antihydrogen, and that potentially could lead to much colder atoms being produced, as long as the antiprotons are far colder, is the charge exchange reaction of Eq. (2) whose cross-section scales with the Ps principal quantum number n_{Ps}^4. By producing and exciting positronium, it is thus possible to produce large amounts of Rydberg antihydrogen, with the additional benefit of having control of its Rydberg state. Contrary to (1), where the velocity of the formed antihydrogen atoms is relatively high due to the requirement of velocity-matching antiprotons to the positron velocity in the positron plasma (much higher for identical temperatures), with implications for trapping (see Fig. 5), the large mass difference between the antiproton and the Ps entails that the kinetic energy of antihydrogen formed via (2) is determined by the antiproton temperature that can be achieved. Note that for $T(\bar{p}) \leq 1K$, the impact of T(Ps) begins to affect $T(\bar{H})$ through the imparted momentum transfer. However, the use of recently developed [37] cryogenic Ps formation targets with Ps velocities as low as 10^4 m/s, equivalent in temperature to that of the Ps formation target, should mitigate even this low momentum recoil.

The scheme successfully demonstrated by the ATRAP collaboration in 2004 [38] (Fig. 4) builds on two consecutive charge-exchange processes, a first step consisting of interacting laser-excited Cs atoms with trapped positrons to form Rydberg positronium, and a second charge exchange process in which part of an isotropically expanding positronium cloud interacts with nearby trapped antiprotons to form Rydberg antihydrogen. In spite of the pulsed nature of the two-step Cs

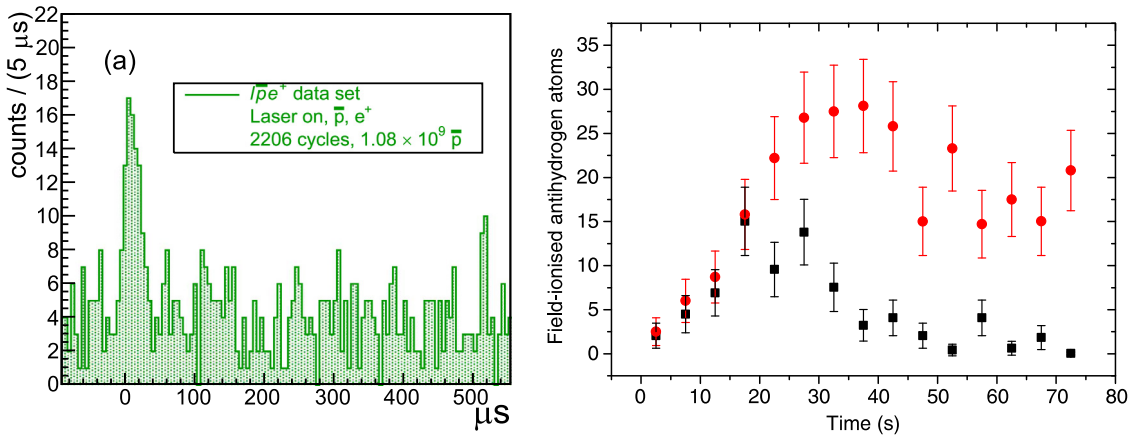

Fig. 3. Left: (a) AEgIS pulsed antihydrogen formation: distribution of the time of annihilation of the formed antihydrogen atoms relative to the time of the Ps excitation laser pulses (t = 0). The excess signal after $t = 0$ is due to pulsed antihydrogen formation and is a convolution of the temporal spread of the time of formation with that of the time of flight of the formed antihydrogen atoms prior to annihilation [36]. Right: $\bar{H}$ formation in the ASACUSA experiment [35]: number of antihydrogen atoms that are field-ionized at an axial distance of 20 cm from the formation region. The axis is that of the anti-Helmholtz coil configuration and of the nested trap, and the minimal principal quantum number for field ionization to occur is $n \sim 39$. Black squares: standard injection of $\bar{p}$ into trapped positrons; red dots: rf-assisted scheme to counteract axial separation of $\bar{p}$ and e^+. Reproduced with permission.

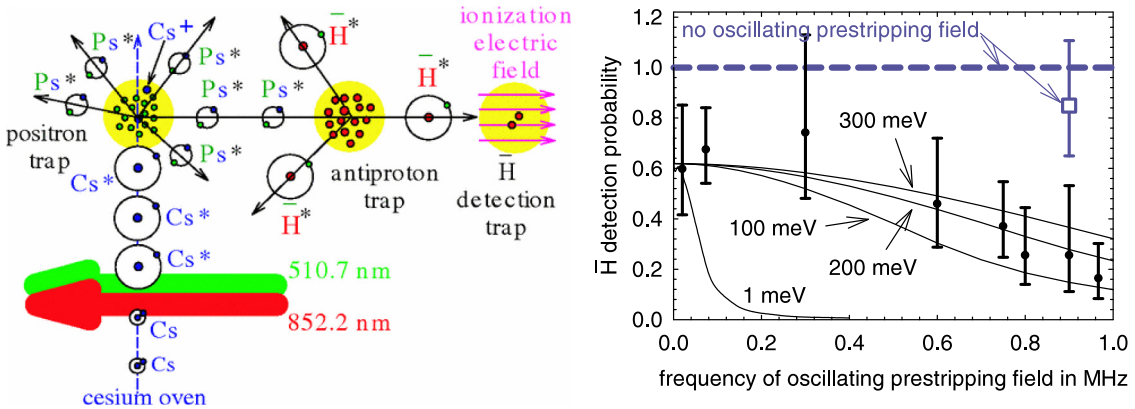

Fig. 4. Left: schematic for laser-controlled $\bar{H}$ production: Cs atoms in a gas jet are excited into Rydberg states via two laser pulses (852.2 nm: $6S_{1/2} \rightarrow 6P_{3/2}$ and 510.7 nm: $6P_{3/2} \rightarrow 37D$); these Rydberg Cs atoms undergo a charge-exchange reaction with trapped cold positrons to form positronium (also in a Rydberg state); as these neutral positronium atoms diffuse, they will undergo a second charge exchange reaction with antiprotons trapped nearby, to form Rydberg antihydrogen [38]. Right: Transmission probability through a pre-field-ionizing oscillating potential, showing that mainly high velocity $\bar{H}$ are formed: 300 meV corresponds to $\approx$ 1000 K [39]. Reproduced with permission.

laser excitation, given the thermal spread of the Cs atoms and their flight path from the point of excitation to the point at which they interact with the positrons, the uncertainty on the time of formation of the atoms is of the order of 100 μs; the employed laser repetition rate of 20 kHz results in a quasi-continuous formation of antihydrogen atoms.

Pulsed formation of antihydrogen atoms was demonstrated in 2018 by the AEgIS collaboration [36]. The formation process also relies on charge exchange, but directly forms positronium via implantation into a nanoporous converter in the vicinity of the trapped antiprotons. The backward-emitted o-Ps is laser-excited via two laser pulses (205.045 nm and 1693 nm) into Rydberg states ($n \sim 18$). These Rydberg Ps traverse the short distance to the antiprotons in O(100 ns), thus resulting in an uncertainty on the moment of formation of the antihydrogen atoms with a FWHM of 80 ns. Given that in (2), the velocity distribution of the produced antihydrogen atoms is determined by the thermal motion of the (cryogenic) antiprotons, sufficient time for potential subsequent laser manipulations of the O(mm^3) cloud of antihydrogen atoms is available. The signal in Fig. 3 (left) corresponding to the time at which the formed antihydrogen atoms annihilate (relative to the time at which the laser pulses excite the Ps atoms formed in the conversion target) is a convolution of the time of formation with the drift time of the formed atoms from the point of formation to the material surface of the trap electrodes on which they annihilate.

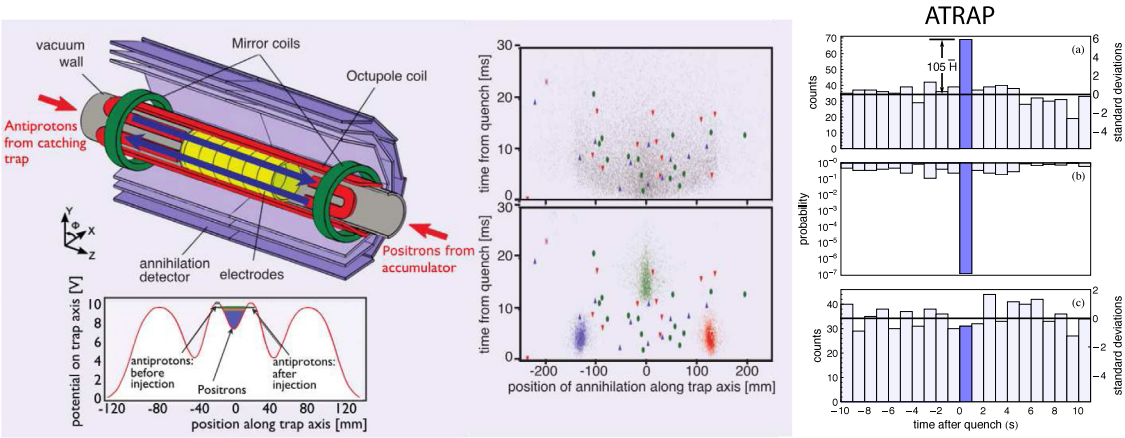

Fig. 5. Trapping of antihydrogen by ALPHA and ATRAP: Left: Antihydrogen synthesis and trapping region of the ALPHA apparatus and nested-well potential used to mix antiprotons and positrons. Center: Measured t-z distribution of annihilations obtained for three (red, green, blue) different experimental conditions (to differentiate trapped $\bar{H}$ atoms from trapped $\bar{p}$'s) during the opening of the ALPHA magnetic trap. Colored symbols are data, the gray dots are simulations for antihydrogen atoms (center, upper plot); the same data are shown below, this time in comparison to expected distributions for antiprotons (tiny colored dots) that could have been trapped instead of $\bar{H}$ atoms, for three different experimental conditions [40]. The color codes are the same for data and simulations. Right: Detected antihydrogen annihilations after trap release at $t = 0$ in the ATRAP experiment. The solid line at 35 counts corresponds to the average cosmic ray counting rate. (a): detected annihilation rate as a function of time; (b): probability that the observed counts in each bin stem from cosmic rays; (c): control sample showing no signal during the trap quench [41]. Reproduced with permission.

2.2. Antihydrogen manipulations

2.2.1. Trapping

Precision experiments on antihydrogen atoms benefit greatly from trapping them, as the ability to spectroscopically induce transitions that remove specific quantum states from the trap is a highly sensitive technique put to excellent use by the ALPHA collaboration (Section 2.3). Antihydrogen atoms, if they are produced in nested electric potential wells (required to mix antiprotons with positrons) at currently achievable temperatures of O(10 K), will only survive for a few μs after being formed before impacting on the walls of the electrodes forming the potential wells and annihilating. It is currently not possible to slow down and cool energetic antihydrogen atoms formed continuously and randomly, and to trap them subsequently.

Instead, trapping antihydrogen atoms relies on forming them inside a (neutral atom) trap, and at energies lower than the trap's potential. A magnetic minimum trap, which relies on the coupling of (anti)hydrogen atoms to magnetic fields via their small magnetic dipole moment can be formed by overlaying a transverse magnetic multipole (quadrupole, octupole) and two axial Helmholz-like coils onto the axial magnetic field that forms part of the antiproton Penning trap. In its ground state, the magnetic moment of the antihydrogen atom is minimal (Rydberg states have a much larger dipole moment) but these are the states that need to be trapped; the well depth for these is 0.76 KT^{-1}. State-of-the-art systems achieve a trap depth of about 1 T in compact devices, and thus of 0.76 K, corresponding to an antihydrogen kinetic energy of 65 μeV.

Even forming antihydrogen atoms in this challenging (magnetic) environment is a recent development. It is only in 2008 that the first antihydrogen atoms were formed in a quadrupolar [42] or octupolar magnetic trap. Furthermore, antihydrogen atoms need to be formed at the lowest possible temperature, in order to trap even a fraction of the formed atoms, which in turn requires – in the case of three-body recombination – the lowest possible positron temperature. In 2010, the ALPHA collaboration reported on the first trapping of such ultra-cold antihydrogen atoms [40] formed via this process, which correspond to a minute fraction of all atoms produced in their trap; in a second paper [43], they furthermore showed that the trapped atoms had decayed into the ground state. Comparable results were also obtained by the ATRAP collaboration [41] in 2012, in spite of much slower trap release time constants.

Through better reproducibility and control of the antiproton and positron plasmas (e.g. sympathetic cooling of e^+ via laser-cooled co-trapped Be^+ ions, as first demonstrated by [44], and now achieved by [45] in view of reducing the temperature at which their $\bar{H}$ are formed), the ALPHA collaboration has continuously improved trapping rates in recent years (currently more than ten atoms per cycle). Equally importantly, they have demonstrated the ability to stack, i.e. continuously accumulate additional atoms into a trap already containing atoms from earlier trapping attempts [46] which has allowed a number of fundamental advances that are discussed in sections 2.2.3 (cooling) and 2.3 (spectroscopy and atom manipulation).

2.2.2. Beam formation

Alternatively, antihydrogen atoms can be studied in flight, the forward boost ensuring sufficient time for spectroscopic measurements or manipulations as the atoms propagate away from the (compact) formation region [47]. Two approaches are being pursued to produce (O(1000 m/s)) antihydrogen beams. The first method, pioneered by the ASACUSA collaboration, relies on continuous formation in a nested trap geometry (similar to that of Fig. 2, center) albeit in a magnetically non-isotropic environment [34] that can focus half (two of the four ground state hyperfine states) of the isotropically-emitted antihydrogen atoms axially, by separating the two spin orientations of the positron by means of an anti-Helmholtz coil-induced magnetic field gradient. The second approach, pursued by the AEgIS collaboration, builds on pulsed formation of antihydrogen atoms in Rydberg states which are either accelerated by synchronized electric field gradients (Stark acceleration) or in which the antiprotons are provided with meV energies axially just prior to formation of antihydrogen [48]. Finally, also trapped antihydrogen atoms can be accelerated by the dipole force of a traveling optical lattice to form a beam, as a recent simulation [49] indicates.

The ASACUSA collaboration has studied the downstream flux of (Rydberg) antihydrogen atoms produced in a close-to-homogeneous magnetic field region in proximity to the magnetic cusp field produced by two Helmholtz coils in anti-Helmholtz geometry. Given the role that the temperature of the positrons plays in the three-body recombination process, the resulting Rydberg antihydrogen atoms are rather fast, with a lower limit of around 1000 m/s for an assumed formation temperature of 50 K. Together with the observation that the lowest lying states of the formed antihydrogen atoms are at $n \sim 15$ [50], this underlines that further steps to reach a flux sufficient for measurement of the ground state hyperfine splitting are required. Indeed, both techniques to achieve colder positron temperatures (e.g. via sympathetic cooling with laser-cooled Be^+ ions [51]) as well as Rydberg de-excitation (via collisional de-excitation in plasmas [52] or stimulated de-excitation [53]) are under active investigation.

Similarly challenging is the development of a pulse-formed beam of antihydrogen atoms: while pulsed formation of isotropically emitted low temperature ($v \sim 1500$ m/s, corresponding to O(100K)) antihydrogen has now been established [36], directionally enhanced emission has not yet been demonstrated, with the additional challenge that the resulting antihydrogen velocity along the beam direction should not exceed ~ 1000 m/s, equivalent to an axial energy of $\sim$ 1meV. This will require not only forming colder ($v \sim 100$ m/s) antihydrogen, but also requires a mechanism by which the antihydrogen atoms are either emitted preferentially in one direction, or are accelerated after formation. One approach for the later is to build on techniques developed to Stark decelerate (and trap) Rydberg hydrogen atoms [54] along a specific direction. These techniques achieve a $\Delta(v)$ of 700 m/s in 5 μs using time-dependent inhomogeneous electric fields and, with the possibility of rapid switching on of such accelerating electric fields, are well matched to pulsed formation. Acting on the low temperature Rydberg antihydrogen atoms immediately after their formation could also rely on the ponderomotive force induced by strong short-pulse laser fields [55].

2.2.3. Cooling

Laser cooling of antihydrogen atoms in multipolar magnetic traps coupled to Penning traps in which these atoms are formed is a daunting undertaking, given the very low numbers of trapped atoms (in comparison to the matter analog of hydrogen atoms), the very limited access and available laser power at 121.6 nm, and finally, the concomitant impossibility of carrying out laser cooling from multiple directions, raising the question of the degree of three-dimensional thermalization in the case of one-dimensional cooling. In spite of these challenges, the ALPHA collaboration has, in a series of refinements that include the recent implementation of a pulsed Lyman-α laser able to drive the 1S-2P cooling transition (see Section 2.3), demonstrated efficient cooling of a sub-sample (their method focused on that half of the trapped sample of antihydrogen atoms in which the spins of the antiproton and of the positron were parallel) of the continuously accumulated antihydrogen atoms in their trap [56] (Fig. 6, right).

Critically, two processes could be combined, since while for some data sets, continuous accumulation of antihydrogen atoms was carried out until a sample of O(1000) atoms was available (several hours), prior to spin selection and subsequent cooling (or heating), again for several hours, the collaboration could also show that continuous application of the cooling laser during the continuous accumulation was not only not detrimental to the accumulation rate, but furthermore resulted in an even lower-energy ensemble than the step-wise approach. Additionally, in spite of only axial laser access, three-dimensional cooling was demonstrated, indicating that the anharmonic magnetic trapping potential resulted in coupling of the motional degrees of freedom of the antihydrogen atoms.

An immediate consequence of the resulting much lower energy trapped antihydrogen sample is a very significant narrowing of the 1S-2S two photon transition with respect to uncooled (but trapped) atoms in the same apparatus, which furthermore provides confirmation of the crucial three-dimensional cooling. Implications go well beyond this simple improvement in resolution, with impacts on determinations of the antihydrogen Lamb shift, fine-structure splitting or hyperfine splitting as both Doppler and transit-time broadenings are reduced, and furthermore, Zeeman broadenings within the anisotropic magnetic field of their multipolar magnetic trap become negligible as the cooled antihydrogen atoms concentrate in the most homogeneous region of the magnetic well. Furthermore, laser-cooling of trapped $\bar{H}$ brings into reach a wide range of novel fundamental measurements and systems (see Section 7.1).

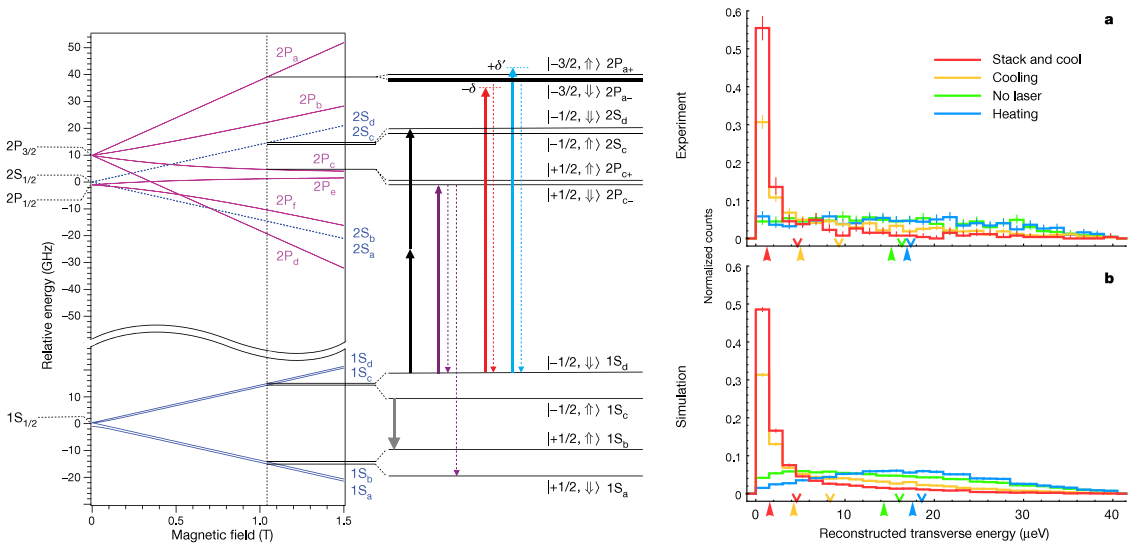

Fig. 6. Left: Level scheme of antihydrogen atoms in a magnetic gradient trap and cooling (red), heating (light blue), probing (purple), 1S-2S spectroscopic two-photon (black) and de-populating microwave (gray) transitions. Right: (a) Reconstructed measured and (b) simulated transverse energy distributions for laser-cooled and laser-heated trapped $\bar{H}$ atoms. For details, see [56]. Reproduced with permission.

2.3. Spectroscopy

One of the main goals of antihydrogen experiments is to carry out precision spectroscopy (Fig. 7, left). For this, two transitions are attractive: the transition between the ground state (1s) and the first excited states (2s) which can only decay via two-photon emission, and has been measured in hydrogen [57] to a few parts in 10^{15}; and the hyperfine transition (HFS) in ground state antihydrogen, which – in hydrogen – has been measured with a relative precision of 10^{-12}, and can potentially be measured – in antihydrogen – with a relative precision of 10^{-7} or better via microwave-based methods pursued both by the ASACUSA and the ALPHA collaborations.

Since 2013, a number of increasingly precise spectroscopic measurements of antihydrogen relying on spectroscopically removing selected trapped antihydrogen atoms from the multipolar magnetic trap have been carried out. The ALPHA collaboration focused first on the (HFS) microwave transition [58,59]. Although the energy levels, and thus their splitting, of the trapped antihydrogen atoms depend on the position of the atom within the magnetic potential well, the field minimum of 1 T ensures that no hyperfine splitting below that of the value at 1T can take place. By exposing trapped antihydrogen atoms to a scan across a range of microwave radiation around this minimum, the ALPHA collaboration was able to induce spin-flips in the trapped atoms, which then – because they were now in an un-trapped configuration – could be detected through their subsequent annihilation. Fig. 7 (left) shows the Zeeman splitting, the spin-flip transition line shapes and microwave scan windows (two possible transitions), and the rate of detected antihydrogen atom annihilations over each window.

Also the ASACUSA experiment [34] has the goal of measuring the ground state hyperfine splitting of antihydrogen, but their approach, based on a spin-polarized beam allowing a measurement in a magnetic-field free region, targets a different combination of transitions between sub-states: the π_1 transition between the (F=1, M_F = -1) and the (F=0, M_F = 0) antihydrogen states, as well as the σ_1 transition between the (F=1, M_F = 0) state and the same (F=0, M_F = 0) state. While the difference between the π_1 and the ((F=1, M_F = 0) → (F=1, M_F = 1)) π_2 transitions is insensitive to coefficients of the Standard Model Extension (SME) effects [4,5], and thus to Lorentz or CPT violating terms, the difference between π_1 and σ_1 is.

Very recently, the ALPHA collaboration also carried out a precision measurement [60] of the 1s-2s transition (Fig. 7, right). Also this measurement relies on selectively depopulating the trapped antihydrogen atom ensemble: after a first excitation of the 2-photon $1S_d$-$2S_d$ transition, the $1S_c$ state is depopulated via microwaves. Atoms excited into the 2*S* state via a two-photon transition can either be photo-ionized through a third photon, or can decay into an untrappable 1*S* state in case of a spin flip. Tallying both losses and numbers of atoms remaining in the $1S_d$ state after subjecting the trapped atoms to laser and microwave radiation allows building a frequency-dependent 'survival' and 'disappearance' curve, thus mapping out the $1S_d$-$2S_d$ resonance. The resulting spectral line agrees with that expected for hydrogen under the same conditions to about 5 kHz out of 2.5×10^{15} Hz.

A third group of spectroscopic measurements (being pursued by both the ALPHA and the GBAR collaborations) focuses on the Lamb shift, the energy gap between the 2S and $2P_{1/2}$ energy levels, stemming from vacuum polarization effects in quantum fluctuations, but is also affected by the details of the (anti)proton radial charge distribution (charge radius), the

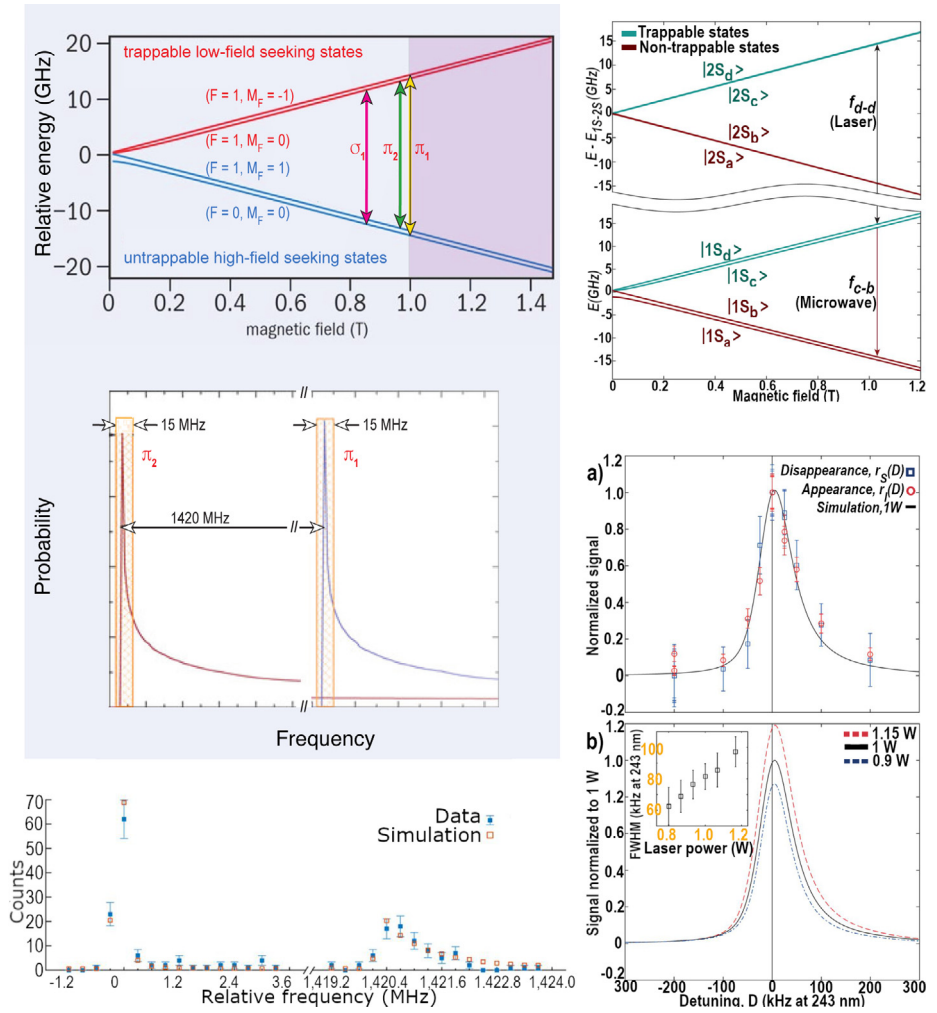

Fig. 7. Left, top: Breit–Rabi diagram of the hyperfine energy levels of ground state antihydrogen. Middle: Spin-flip transition line shapes and microwave scan windows for the π_1 and π_2 transitions in [58]; the subsequent measurement [59] used narrower scan windows. Bottom: Number of detected antihydrogen annihilation events (filled blue squares) by the ALPHA experiment as a function of microwave frequency. The expectations, scaled to match the total number of observed events, from the simulation for hydrogen in their trap are also shown as open red squares. Details can be found in [59]. Right, top: Calculated energies (hydrogen) of the hyperfine sublevels of the 1*S* (lower) and 2*S* (upper) states, plotted against magnetic field strength. The centroid energy difference $E_{1S-2S} = 2.4661 \times 10^{15}$ Hz has been suppressed on the vertical axis. The vertical black arrow indicates the probed two-photon laser transition (frequency f_{d-d}); the red arrow illustrates the microwave transition used to remove the $1S_c$ state atoms (frequency f_{c-b}); Right, bottom, (a): The complete dataset, scaled as described in [60]. The simulated curve (normalized to the data at zero detuning) is for a stored cavity power of 1 W. "Appearance" refers to annihilations that are detected during laser irradiation; "disappearance" refers to atoms that are apparently missing from the surviving sample. (b) Three simulated line shapes (for hydrogen) for different cavity powers to illustrate the effect of power on the size and the frequency at the peak. The width of the simulated line (FWHM) as a function of laser power is plotted in the inset. For details, see [60]. Reproduced with permission.

weak nuclear force or potential BSM phenomena. Achieving an uncertainty of one part in 10^4 would allow determining the charge radius of the antiproton to 10% [61]. Additionally, the measurements involved in extracting the Lamb shift also allow determining the Rydberg constant R_∞, and are of more general interest in that they allow testing Lorentz and CPT symmetries [62].

The Lamb shift can be determined from a series of precision spectroscopic measurements of transitions into the 2S and 2P states, as are being carried out in hydrogen, where two-photon measurements of the 1S-2S [63] and the 1S-3S [64] transitions (but also others) to 10^{-12} or better are combined with the aim of deducing R_∞ and the proton radius. Spectroscopy of the same sets of transitions to the same precision with trapped antihydrogen should be feasible, although the schemes may need to be adapted for some transitions to account for the fact that spin flip inducing transitions will result in losses of trapped atoms in the course of the measurement.

A similar approach was carried out for antihydrogen by the ALPHA collaboration, who measured the 1S-2P Lyman-α transitions in antihydrogen [65], determining their frequencies (in a magnetic field of 1 T) to a precision of 16 ppb. From

this, they infer the zero-field fine-structure splitting ($2P_{1/2} - 2P_{3/2}$) in antihydrogen. In combination with their earlier precision measurement of the 1S-2S transition [60], they obtain a value for the Lamb shift in antihydrogen ($2S_{1/2} - 2P_{1/2}$) that is consistent (within its 11% error) with theory.

An alternative (direct) measurement of the Lamb shift pursued by the GBAR collaboration relies on the availability of a beam of $\bar{H}$ in the metastable 2S state [61,66]. By passing this beam through two microwave cavities, a first one to select the appropriate hyperfine state, and a second one to induce a $2S \rightarrow 2P$ transition; similarly to the same approach that was applied to hydrogen [67], de-excitation of the 2P state (τ = 1.6 ns) to the ground state can then be determined as a function of the microwave frequency.

2.4. Gravity

Tests of another fundamental symmetry, the weak equivalence principle (WEP), are also under preparation; violations of this symmetry in matter–antimatter systems are allowed, for example, in a specific effective quantum field theory, the isotropic parachute model [68]. While experiments with the goal of measuring the behavior of matter and antimatter in the Earth's gravitational field have been contemplated before, the weakness of the gravitational interaction, and the impossibility of sufficiently shielding remnant electric and magnetic interactions for charged (anti)particles has hindered their realization. Several groups have thus proposed experiments using neutral antihydrogen atoms as gravitational probes.

Indirect limits on potential weak equivalence principle violations can be obtained via searches for differences in the q/m ratio of protons and antiprotons. The obtained limits on these ratios at the ppt level as measured in the ATRAP [69] and BASE [70] experiments are direct tests of CPT; they can however be reinterpreted as limits on WEP violations if CPT conservation is assumed. Comparable constraints on any possible anomalous matter–antimatter gravitational interactions at the level of parts in 10^7 from a combined analysis of clock-comparison, torsion balance and matter–wave interferometric experiments, as well as of internal bound kinetic energies of nucleons in nuclei [62,71], however lie well beyond the reach of the first generation of experiments with antihydrogen atoms which are aiming at sensitivities in the % to ‰ level. Future developments building on e.g. light pulse interferometry could however reach a sensitivity at the ppm level [72].

The first such experiment (currently working through the list of required technical developments) is the AEgIS/AD-6 experiment [48]. It aims to produce a moderately focused pulsed horizontal beam of antihydrogen atoms, whose parabolic trajectory can be measured via a high resolution annihilation detector (with a required spatial resolution of $\sim$ 1 μm, two possible technologies are under investigation: a silicon-photographic emulsion hybrid; and a silicon-high resolution MCP hybrid). Two periodic gratings (e.g. a classical moiré deflectometer [73]) will be employed to produce a spatially modulated distribution of transmitted atoms. Since the vertical shift of the periodic pattern depends on the time during which a set of mono-energetic atoms fall, each atom's velocity will be determined by forming all atoms simultaneously (through charge exchange between laser-excited positronium and ultra-cold antiprotons) and measuring the arrival time of each atom (in the annihilation detector) together with its vertical position.

A second method has been proposed by the GBAR collaboration [74]: by interacting a low energy beam of antiprotons with a high-density cloud of positronium atoms, a dual charge exchange process (as described in chapter 2.1) first forms ground state antihydrogen, and subsequently, the bound $\bar{H}^+$ ion, a stable and positively charged antihydrogen ion [75]. In order to enhance the formation cross section, laser-exciting the positronium from the ground state to an excited state is beneficial [76–78]: the production rate of the antihydrogen ion close to the reaction threshold is noticeably increased with respect to ground-state Ps. This formation mechanism will be discussed in more detail in Section 6. Trapping and interacting this positive anti-ion with other laser cooled (matter) cations (e.g. Cs^+) allows a first pre-cooling before a final cooling step with laser-cooled Be^+ to μK is carried out [79]. In a last step, the $\bar{H}^+$ will be laser-ionized; the neutral $\bar{H}$'s free fall time from the trap to a detector measures its gravitational behavior [80]. Optimization of the sensitivity of the future measurements to g by careful analysis of the timing of these expected events is currently being explored [81,82].

Finally, trapped antihydrogen atoms can also be released, and – if they are sufficiently cold – their subsequent free-fall behavior can be investigated. While first attempts [83] by the ALPHA experiment did not yet have the necessary sensitivity — at several 100 mK, the velocities of the (neutral, uncooled) trapped atoms are still far too high — this method being pursued with the dedicated ALPHA-g apparatus may well reach the required sensitivity, if laser cooling on the 1s-2p transition (recently demonstrated in antihydrogen by the ALPHA collaboration [84] and discussed above) is applied to the trapped antihydrogen atoms. This last approach is the most advanced among the three attempts, and furthermore offers a path towards future, more precise measurements via, e.g. atomic fountains of antihydrogen atoms [85] or other precision techniques [86].

2.5. Other antihydrogen investigations

While baryon (B) and lepton (L) number conservation is well established, a number of models [87,88] allow the possibility of $\Delta(B) = 2$ or $\Delta(B) = \Delta(L) = 2$ processes, in which neutron–antineutron or hydrogen–antihydrogen oscillation would occur, and which evade limits stemming from the non-observation of proton decay. A recent paper [89] has revisited bounds on the occurrence of the later, which come mainly from searches for γ rays from the annihilation of

any appearing $\bar{H}$ in the interstellar medium. They update a previous bound that neglected the effect of elastic collisions, and find, using the most recent observational data, that $|\delta| \leq 6 \times 10^{-17}$ s^{-1}, where $|\delta|$ is the oscillation parameter between H and $\bar{\text{H}}$.

Potential laboratory tests will struggle to compete: the same paper explores a Gedanken experiment with falling hydrogen atoms, and finds that to reach even a much less stringent bound than the above value based on γ-ray observations by the Fermi Large Area Telescope [90] (which determined the diffuse γ-ray flux and compared it with the expected cosmic ray-induced γ-ray flux) of $|\delta| \leq 10^{-16}$ s^{-1} would require observation of 10^8 mol of atomic (anti)hydrogen during 1 s of free fall.

3. Protonium and antiprotonic deuterium

The simplest antiprotonic atom is protonium, a bound state of an antiproton with a proton, often denoted as Pn. The 1s binding energy and radius are of the order of 12 keV and 50 fm, respectively. These atoms were historically formed by slowing down antiprotons (by ionization loss), initially in liquid or high pressure gaseous hydrogen, and later, in a dilute gas of hydrogen. Once the antiproton is (almost) at rest, it will replace the electron of the hydrogen atom, in an orbit whose radius is that of the first Bohr radius of hydrogen, approximately 5.3×10^{-9} cm. The protonium thus formed will have a large angular momentum, l, and a principal quantum number, n, of about $(m_p/m_e)^{1/2} (\sim 45)$, where m_p and m_e are the mass of the proton and of the electron [16]; for a distribution of n values, see fig. 2, in [15]. During de-excitation, (n,l) quantum numbers are reshuffled: for formation of protonium in liquid hydrogen, Desai [16] showed that annihilation of the proton–antiproton system would take place essentially exclusively from states with zero angular momentum (albeit with possibly high principal quantum number). This prediction depends on the likelihood of Stark mixing, however, and so is strongly density dependent [91]: protonium formation and cascades in low density hydrogen (requiring of course low-momentum antiprotons) would be expected to contribute annihilations from p (or higher angular momentum) states, and indeed, population of (and annihilation from) the 2P state of protonium was observed [92] for formation of protonium in a low density gaseous hydrogen target. Many aspects of the cascade of these (and other) exotic atoms have been explored in more detail in a series of papers published in the proceedings of a dedicated conference [93].

Stark mixing can be completely avoided if protonium is formed in vacuum; this occurs occasionally (albeit uncontrollably) through the interaction of trapped antiprotons with a very dilute population of H_2^+ molecular ions co-trapped together with positrons [18]. The process, which results in $n \sim 68$, $l \leq 10$ protonium with lifetimes of O(1 μs), is then:

$$\bar{p} + H_2^+ \rightarrow Pn(n, l) + H \tag{5}$$

A more interesting production scheme which offers full control and potentially much longer lifetimes is based on the technique for pulsed production of antihydrogen via resonant charge exchange. In this case, antiprotons and H^- ions are co-trapped and electron-cooled; the Pn formation reaction is initiated by first photo-ionizing the trapped H^-, and then immediately exciting it into a Rydberg state via a two-step excitation pathway, first from $1S_0$ to $2P_1$ via a 121 nm pulse, and immediately afterwards from $2P_1$ to nS (or nD) via an infrared laser pulse, e.g. to $n = 30$ [94], a process that can easily be adapted to pulsed formation of other antiprotonic Rydberg atoms (e.g. antiprotonic deuterium or antiprotonic lithium) or molecules, starting from co-trapped antiprotons and the corresponding anionic species. These will be discussed in subsequent sections of this review. Interestingly, a quantum–classical hybrid approach [95] finds that at low collision energies, for excited hydrogen atoms (already for n=2), the protonium formation cross section is significantly enhanced over the simple Langevin cross section.

Note that this is the only neutral atom with baryon number zero (to be compared to the purely leptonic positronium atom Ps) than can be experimentally realized for the foreseeable future. In analogy to searches for mirror matter [96] through putative oscillations of the neutral purely leptonic atoms Ps [97], of μe [98], or of neutrons [99] into their mirror matter counterparts, it is tempting to consider the possibility of searching for oscillations of protonium into mirror protonium. It is however not clear whether the analogous couplings that are relevant in the case of Ps or neutrons can occur in this case. Detection of such a state would have to rely on the detection of X-rays from the decay of protonium, emitted prior to its oscillation into its mirror counterpart, and the absence of a visible annihilation signal of mirror-matter protonium into mirror matter mesons.

3.1. Spectroscopy

The energy levels of deeply bound (ground state, first few excited states) of protonium are very sensitive to strong-interaction contributions to the standard electromagnetic potential, as well as to contributions stemming from finite-size effects and from the anomalous magnetic moment of the antiproton, and there is a close link between the level shifts and scattering amplitudes [100,101]. Furthermore, the lifetime of these states is reduced because of the presence of the annihilation channel, resulting in a broadening of the X-ray transitions.

The experimental investigation of transitions relies on detection of the fluorescence X-rays, to which however additional X-rays from the acceleration of charge in the annihilation process (inner Bremsstrahlung [102]) contribute, which can furthermore interfere with the transition lines [103]. Separating the level substructures of protonium is

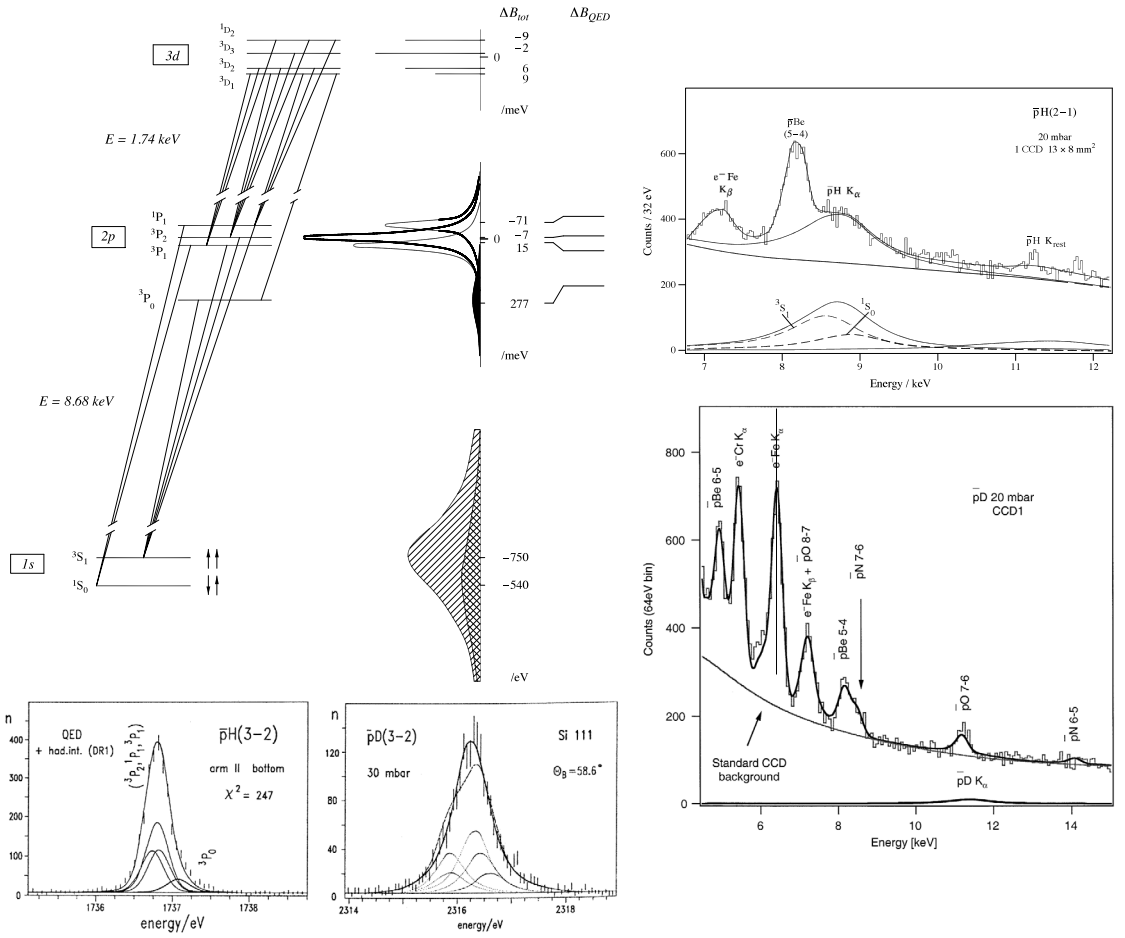

Fig. 8. Left: Top: Low-lying energy levels and transitions in $\bar{p}p$ (from [11]). Energy shifts (ΔB_{tot}) and widths from an optical potential model [104]. Bottom: experimental Balmer-α X-ray spectrum for $\bar{p}p$ along with the hyperfine decomposition. For explanations of the fits, see [105]. Right: Top: X-ray spectrum for $\bar{p}p$; the K_α transition is indicated by the solid line at the bottom of the figure (from [11]); Bottom: Lyman-α transitions of $\bar{p}d$ [106]. Reproduced with permission.

hindered on one hand by the achievable experimental resolution of fluorescence detectors, on the other by the strong-interaction induced level broadenings, and finally, by the cascade-dependent level populations. Fig. 8 illustrates the level broadenings and shifts relative to a purely QED-based calculation.

The corresponding level shifts and annihilation-induced level broadenings, particularly of transitions into the 1*s* state, were studied with increasing energy resolution at LEAR, first with a gaseous detector (both in the absence [92] and the presence [107] of inner Bremsstrahlung), with $\Delta(E)/E \sim 10\%$, and subsequently with a higher resolution Si(Li) X-ray detector [108,109] as well as a crystal spectrometer coupled to CCD's [11,103,105,106], with $\Delta(E)/E \sim 10^{-4}$. Spectra in [108] are complex, with a number of background X-ray contributions from antiprotonic atoms formed with contaminant gases (O_2, N_2), and while a value for both the energy shift and level broadening for $\bar{p}p$ K-X-rays is extracted, and the K_α ($2\rightarrow 1$) transition identified, in the $\bar{p}d$ system, because of the more frequent annihilation from p levels as compared to $\bar{p}p$, no clear evidence was found for the ground state transition (which corresponds to 1% of the 2P population in $\bar{p}p$).

Observation of this transition, as well as a splitting of the $\bar{p}p$ ground state hyperfine levels, was made possible by the higher resolution and sensitivity of the PS207 cyclotron trap (Fig. 8). For the ground state, the spin and isospin dependence of the strong interaction determines the shift and broadening of each of the two K-lines corresponding to transitions into one of the $^3S_1$ or $^1S_0$ hyperfine states. While this splitting could indeed be observed for $\bar{p}p$, this was not possible in $\bar{p}d$ due to the more than 10-fold suppression of the ($2\rightarrow$ 1) transition into the ground state in comparison to $\bar{p}p$, as well as experimental challenges stemming from description of the background shape and $\bar{p}$O contamination. The effect of the nuclear polarization — the dipole in the extended charge distribution of both nucleus and $\bar{p}$ induced by the electromagnetic interaction — on the energy shift of the 2p level is negligible in protonium; in $\bar{p}$d, the 3d-2p transition energy is more strongly shifted (by −6.6 meV) due to the large quadrupole moment of the deuteron [110]. Nonetheless, the comparison of $\bar{p}p$ with $\bar{p}d$ highlights a number of interesting differences:

- the broadening of the ground state is unexpectedly the same, with a line width of 1keV; confirmation would require a renewed measurement with an energy resolution of $\Delta E/E \sim 1\%$ at 10 keV or better, but even more importantly, with greatly improved statistics, both to separate the two hyperfine components in $\bar{p}p$ as well as to confirm the signal in $\bar{p}d$.
- for the $\bar{p}p$ 2P levels, the average shift of the (2^3P_2, 2^2P_1 and 2^3P_1) levels is compatible with zero, while the 2^3P_0 state is shifted by (137 ± 28) meV, supporting the presence of an attractive isoscalar tensor interaction [105] (as predicted by the meson exchange model [101,111])
- for the five $\bar{p}d$ 2P sublevels, the average hadronic shift of (-243 ± 26) meV is repulsive [105,112], as predicted [113]. The splitting of the sublevels cannot be resolved and is only observed through the overall fit to the measured distribution.
- as expected, the 2P levels are significantly more shifted in $\bar{p}d$ than in $\bar{p}p$. In the absence of better data on the ground state hyperfine splitting, this is the only (model-dependent) source of information on $\bar{p}d$ hyperfine splitting, with the caveat that the width of this transition is much larger than the expected splitting. The $\bar{p}p$ system thus remains the only one where 2p hyperfine components are accessible.

At this point, a re-measurement of the various transitions, particularly in $\bar{p}d$, with a five-fold improvement in resolution and with increased statistics would be desirable, on one hand to confirm the extracted hyperfine splittings, and on the other to establish the presence and splittings of transitions into the ground state, both in $\bar{p}p$ and in $\bar{p}d$ (and possibly in $\bar{p}t$). If the same technique as that used by PS207 were used, a continuous antiproton beam of the order of 10^5/s would be required, which however will not be available in the foreseeable future. Instead, if improvements in X-ray detection technologies would allow achieving an energy resolution of $\Delta(E)/E \leq 10^{-4}$ at 2 keV, or $\leq 10^{-2}$ at 10 keV, but with a high detection efficiency, then trap-based approaches might become feasible. This is motivated by the goal of reaching sufficient precision on the values for the spin-averaged shifts and widths to become sensitive to the possible presence of decay channels into close-to-threshold $\bar{N}N$ bound states [100], for which a better decomposition of the hyperfine structure is necessary. This requires, in addition to improved resolution and statistics, also reduced systematics, inter alia in form of a better knowledge of the background shape.

Spectroscopy of states much earlier in the cascade, between Rydberg levels, provides an additional rationale to revisit protonium and $\bar{p}d$: from the spectroscopy of protonium, it is possible to improve the proton to electron mass ratio, but in contrast to precision spectroscopy in $\bar{p}$He (see the following section), without referring to the results of three-body theoretical calculations. If a comparably high precision as in $\bar{p}$He can be reached, for example via the scheme proposed by Hayano [114], it should become possible to also resolve and study in detail the protonium hyperfine structure, additionally opening the door to measuring the Rydberg constant with antiprotons. Certainly, for protonium formed in vacuum, the absence of Stark quenching means that only radiative transitions between Rydberg levels can occur, leading to very long (10's of μs) lifetimes [114]).

Finally, it is tempting to consider whether measurements of a (generalized, i.e. between nS and nP levels) Lamb shift in $\bar{p}p$ could be feasible via direct laser-stimulated transitions, similarly to the case of muonic [115] or pionic [116] atoms, even though it is the absence of nuclear reactions in the former that its metastability is due to. Furthermore, annihilation of antiprotonic atoms from nS states, even for highly excited atoms, is very rapid. The specific laser frequency required to drive the $nS - nP$ transition in $\bar{p}p$ will depend on the specific level n, which is furthermore constrained by lifetime considerations: with a lifetime of the $2P$ state of $\bar{p}p$ of $\sim 10^{-14}$ s (in contrast to muonic hydrogen, where the ns (n>1) states are metastable), and an n^3 dependence of this lifetime, tagging a transition into an nP state prior to firing a laser will require lifetimes of O(10 ns), and thus focusing on $n \geq 100$. In Lamb-shift measurements in these exotic atoms, contrary to non-exotic atoms, such as antihydrogen, the dominant contribution comes from vacuum polarization effects, which will however decrease with increasing n. It is thus indeed the $2S - 2P$ splitting, with a value of O(eV), that is the most interesting to attempt to measure. A possible scheme could be to tag transitions into the $2S$ and the $2P$ states through the corresponding fluorescence X-rays. While 98% of atoms reaching the $2P$ state annihilate, detecting the K_α transition into the ground state guarantees that the $2P$ state was reached, while annihilations from the $2S$ state will never be accompanied by this 9 keV photon; an enhancement of the K_α signal as a function of an appropriate laser pulse (triggered by an earlier radiative transition in the cascade) would signal a modification of the relative $2S$ and $2P$ populations.

4. Antiprotonic helium

The metastability of antiprotonic helium was discovered as a delayed annihilation component ($\tau \sim$ 3–4 μs) in antiprotons injected into liquid helium [117], leading to the very rapid implementation and measurement of laser-induced transitions in these long-lived $\bar{p}He$ atoms [118] only 3 years later by the PS205 experiment at LEAR. These metastable states are due to the particular characteristics of He with respect to other atoms: the trapped antiprotons can, in a few percent of the cases, be captured in nearly circular Rydberg orbits (n $\sim$ 38), in which case Auger emission of the second (deeply bound) electron is suppressed.

The technique developed by PS205 [119] is based on injecting a large number of antiprotons into gaseous helium. While most (short-lived) states will annihilate within few ns, some long-lived metastable states may be populated and

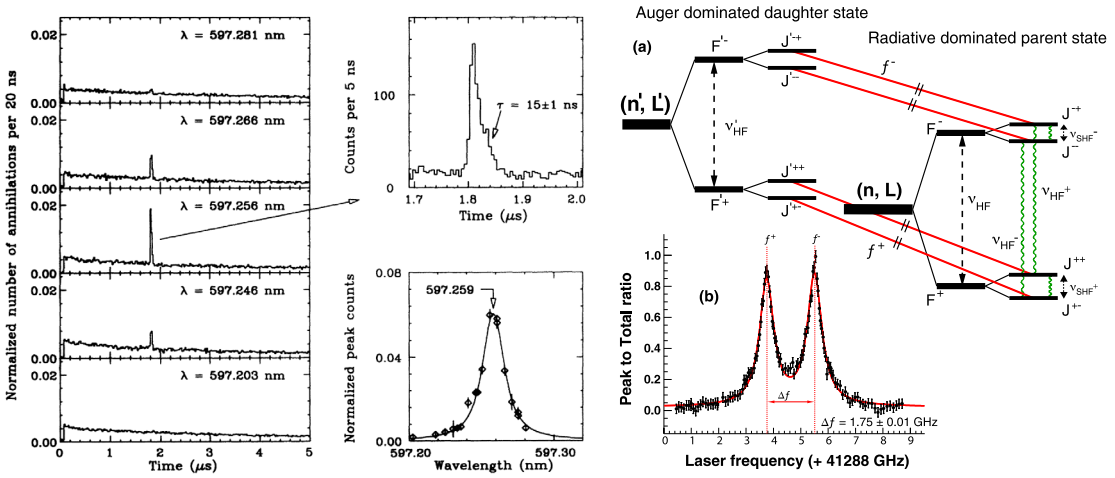

Fig. 9. Left: Observed time spectra of delayed annihilation of antiprotons with laser irradiation of various vacuum wavelengths near 597.2 nm, normalized to the total delayed component [118]. Spikes due to forced annihilation through the resonance transitions are seen at 1.8 μs. Upper middle: Enlarged time profile of the resonance spike. A damping profile with a time constant of 15 ± 1 ns is observed. Lower middle: Normalized peak count versus vacuum wavelength in the resonance region, showing a central wavelength 597.259 ± 0.002 and a FWHM 0.018 nm. Right: (a) Schematic view of the level splitting of $\bar{p}\mathrm{He}^+$ for the $(n, l) \rightarrow (n-1, l+1)$ electric dipole transitions [125]. The laser transitions f^+ and f^-, from the parent to daughter states, are indicated by straight lines and the microwave transitions, between the quadruplets of the parent, by wavy ones. For this experiment $(n, L) = (37, 35)$ and $(n', L') = (38, 34)$. (b) Laser resonance profile demonstrating the two sharp peaks and HF laser splitting $\Delta f = f^- - f^+$. Although there are four SHF laser transitions only the HF transitions were resolved in this experiment.
Source: Reproduced from [118,125] with permission.

can be probed via a delayed laser pulse which – if it corresponds to a transition energy from a populated meta-stable state into a short-lived state – will lead to a momentary increase in the annihilation rate (Fig. 9). More specifically, the induced transition is into a state from which Auger emission of the remaining electron can again take place, resulting in a high-n, low-l state of the antiproton, which thus has a significant overlap with the nucleus, and can consequently rapidly annihilate.

The significant advance over direct measurements of the emitted X-rays is that the precision is now limited mainly by the external laser system applied to stimulate the transitions. In addition, however, control over transitions allows selective population and depopulation of states, providing access to a range of transitions (e.g. hyperfine splittings) that are inaccessible to fluorescence-based observations. In a series of improvements of their apparatus and technique (frequency combs, doppler-free two-photon spectroscopy, low density and cold targets), the PS205 experiment (and the successor experiment AD-3/ASACUSA) have improved the knowledge of the transitions by several orders of magnitude, now reaching ppb precisions. In parallel, the crucial theoretical treatment of transition frequencies (now to $O(\alpha^7)$) of the $\bar{p}He$ system has kept pace [120–122], having now reached relative precisions at the 10^{-10} level.

A number of challenges have been overcome by the ASACUSA collaboration to carry out spectroscopy at such a precision: buffer gas cooling of formed $\bar{p}\mathrm{He}^+$ atoms with cryogenic helium gas [123]; going from single-photon transitions to two-photon spectroscopy of non-linear transitions $(n, l) \rightarrow (n-2, l-2)$ [124]; or incorporating microwaves to induce a laser-microwave-laser triple resonance which allowed the ASACUSA collaboration to study the hyperfine structure of the (n, l) = (37, 35) state of $\bar{p}^4\mathrm{He}^+$. This later resulted in a measurement to 0.3% of the magnetic moment of the antiproton [125] (subsequently superseded by direct measurements of antiprotons in traps), in agreement with the corresponding value for the proton, and thus with CPT conservation, as are similar measurements with $\bar{p}^3\mathrm{He}^+$ [126].

Precision spectroscopy of this antiprotonic atomic system also allows a precision comparison of the charges of a particle and its antiparticle: different functional dependencies of the observables (i.e. the Rydberg constant of the exotic atom, and the cyclotron frequency of trapped negative particles) allow factorizing charge and mass. A test to 10 ppm of the equality of the charges and masses of antiprotons and protons [127] combines measurements of transitions in antiprotonic atoms and of the cyclotron frequencies of trapped (anti)protons [69,128], and is limited only by the precision achievable in the exotic atoms' transitions. While these were initially observed via fluorescence [129], leading to a relative uncertainty on the antiproton mass of 5×10^{-5}, precision laser spectroscopy of $\bar{p}He^+$ (currently reaching a relative precision of $\sim 10^{-10}$) has dramatically improved these CPT tests in recent years.

Similarly, fitting eight transitions in $\bar{p}^4\mathrm{He}^+$ and five transitions in $\bar{p}^3\mathrm{He}^+$, all of which exhibit some degree of sensitivity to $m_{\bar{p}}/m_e$, this ratio was determined to be $m_{\bar{p}}/m_e$ = 1836.1526734(15) [130], in excellent agreement with the corresponding value for protons of $m_p/m_e = 1836.152673346(81)$ as determined in a Penning trap experiment comparing cyclotron frequencies between protons and highly charged $^{12}\mathrm{C}^{6+}$ ions [131], respectively between electrons and highly charged $^{12}\mathrm{C}^{5+}$ ions [132]. With recent calculations of the theoretical transition frequencies ($O(\alpha^7)$) at the level of 0.1

Table 2
Spin-averaged hadronic shifts ϵ and level broadenings Γ in $\bar{p}^3$He and $\bar{p}^4$He compared to theoretical predictions. The 2p width was measured directly with semiconductor detectors as a line broadening. The 3d-level broadening is determined from the intensity balance of the (nf – 3d) and the (3d – 2p) transitions and the radiative width of the 3d state. From [11], reprinted with permission, and updated with [138].

	ϵ_{2p}/eV	Γ_{2p}/eV	Γ_{3d}/meV	Reference
$\bar{p}^3$He				
Experiment	-17 ± 4	25 ± 9	2.14 ± 0.18	[139]
Optical potential fit	-6 ± 1	24 ± 2	1.30 ± 0.15	[140]
Multiple scattering	-17.3	42.1	2.16	[141]
Density-folded optical potential	-12	33		[138]
$\bar{p}^4$He				
Experiment	-18 ± 2	45 ± 5	2.36 ± 0.10	[139]
Optical potential fit	-8 ± 1	25 ± 2	1.67 ± 0.16	[140]
Multiple scattering	-18.2	40.4	2.46	[141]
Density-folded optical potential	-19	42		[138]

ppb accuracy in H_2^+, HD^+ and antiprotonic helium [120,121], and further improvements in the theoretical precision being expected, attempts at even more precise measurements by the ASACUSA and BASE collaborations should allow improving the knowledge of $m_{\bar{p}}$ and of $q_{\bar{p}}$ by another order of magnitude (or more). This development is driven by the availability of a more intense and lower energy ensemble of antiprotons from the Extra Low Energy Antiproton Ring (ELENA), possibly allowing to resolve weak $\bar{p}He^+$ transitions between metastable states of smaller natural width [130].

These precision spectroscopic measurements can also be used to constrain exotic spin-dependent interactions between matter and antimatter [133]. Heretofore undiscovered spin-0 or spin-1 bosons can mediate exotic spin-dependent interactions between standard model particles. A comparison between theoretical calculations and spectroscopic measurements of the hyperfine structure of antiprotonic helium allow searching for, and putting constraints on, exotic spin- and velocity-dependent interactions between electrons and antiprotons.

Naturally, searching for further transitions in $\bar{p}$He also allows shedding light on questions of relevance to molecular dynamics, such as commonalities between metastable and Rydberg levels in the diatomic beryllium molecule and the antiprotonic helium atom [134]. In a similar manner, searches for "frozen-planet" resonances in antiprotonic helium, states characterized by an excited electron and a strongly localized $\bar{p}$ at a large internuclear distance from the He^+ [135], can be carried out. Contrary to the usual configuration with the electron of the $\bar{p}$He atoms in the 1s state and the $\bar{p}$ in $n \sim 38$ (with a radial extension of around 1 a.u.), such "frozen-planet" configurations correspond to an electron in a nearly hydrogenic maximally polarized excited Stark state with $n \geq 5$, while the antiproton is confined in a potential well at $R \sim 100$ a.u. In spite of the remoteness of the outer well in these "frozen planet" configurations, it apparently supports a large number of resonances. Forming such a state is challenging, but two possibly feasible pathways were proposed by the authors of the concept [136]. The first builds on the collision of a cold antiproton with a doubly-excited He atom which captures the antiproton in lieu of the outer electron; the second starts from the interaction between a suitably excited singly charged He ion and cold antiprotons.

If the cascade is on the other hand allowed to proceed freely, then the second electron will eventually be Auger-ejected as well, at which point the further de-excitation steps will be determined by the likelihood of the antiprotonic He ion $(\bar{p}\mathrm{He})^+$ undergoing collisional processes with the surrounding He atoms, leading to He-density dependent (n, l) distributions. Annihilation occurs from low-lying S, P or D states, with the relative population depending on the density-dependent de-excitation process.

Of particular interest here is the sensitivity of these low-lying states to the strong interaction, similarly as for protonium and antiprotonic deuterium (see Fig. 8), which allows using the X-ray data to construct and constrain the interaction potential. A number of approaches (Table 2) are able to reproduce the measured shifts and level broadenings for both isotopes of antiprotonic helium. From this, it becomes possible to predict the interaction of antihydrogen with helium [137], as a specific case of atom–antiatom interactions. This is somewhat similar to the above "frozen-planet" states, although at much smaller internuclear separation. For $\bar{H}$-He configurations with $J > 0$, the angular momentum barrier between $\bar{H}$ and He will effectively block the nuclei from overlapping, and consequently annihilation is strongly suppressed. Instead, these configurations will decay through rearrangement of the constituents into (e^+e^-) and $(\alpha\bar{p}e^-)$ on relatively long timescales, forming intermediate $\bar{H}$-He systems. Jonsell et al. [137] find that the lifetime of these states increases with J because the barrier becomes more prominent when the angular momentum repulsion is added. The longest lifetime, estimated to be 0.1 ns, is found for the $J = 3$, $\nu = 37$ state (where ν is the number of nodes of the wave function).

5. Antiprotonic atoms (N > 2)

Of course, antiprotonic atoms with heavier nuclei (the special case of antiprotonic helium has been discussed above) have also been formed, to date by injecting antiprotons in gases, liquids or solids. With the exception of antiprotonic

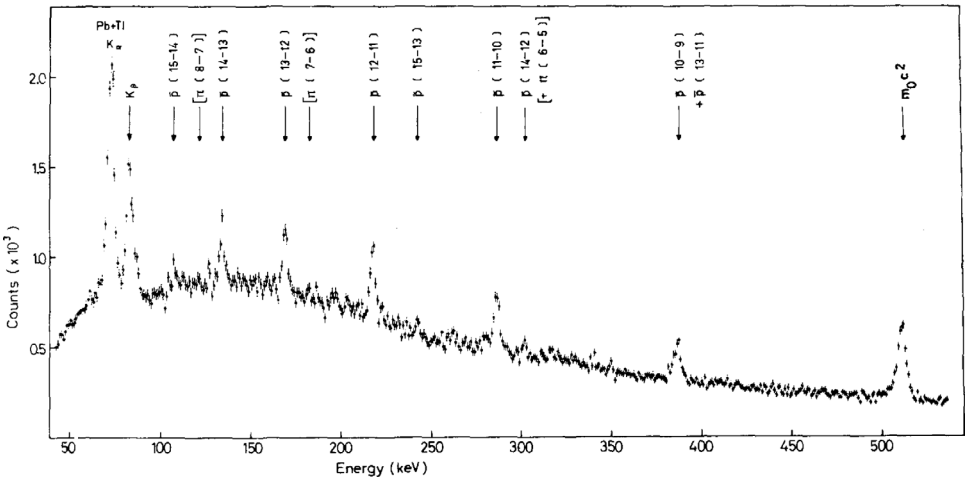

Fig. 10. X-ray spectrum of the first antiprotonic atom to be observed: $\bar{p}-^{81}$Tl obtained from 14×10^6 stopped antiprotons measured with a 10 cm^3 Ge (Li)-detector [143]. Reproduced with permission.

helium (and possibly of antiprotonic lithium, see below), antiprotonic atoms are short-lived, and – in their lowest lying levels – are ideal probes of strong interaction effects.

The strong interaction starts becoming significant for deeply bound or low angular momentum states and dominates once annihilation takes place and radiative transitions no longer occur; the corresponding $n^{annihilation}$ lies between $n = 1$ for $\bar{p}$H and $\bar{p}$D and $n = 9$ for $\bar{p}$U.

The full cascade from $n^{capture}$ to annihilation occurs on timescales of $10^{-9} \sim 10^{-12}$ s [142], except in the case of light elements at very low pressures (and thus suppressed Stark mixing due to interactions between antiprotonic atoms and the surrounding atoms). This picture is greatly modified in the case where the antiproton replaces an electron in a Rydberg state, rather than in the outermost electron shell, since in that case, due to the absence of overlap between the antiproton and the inner electron cloud, only (very slow) radiative transitions can take place. In those systems, the resulting lifetimes can range from μs to tens of ms.

5.1. Historical context

Atomic physics with antiprotons at CERN began with the first observation of antiprotonic atoms in 1970 [143], also providing the first spectroscopic measurement of the antiproton mass. Fig. 10 shows the X-ray spectrum produced by stopping 14×10^6 antiprotons in a Tl target, and illustrates the richness of structures that these systems provide. Comparison between the measured and calculated transitions allowed the authors to give a 68% CL upper limit on any mass difference between protons and antiprotons of ($|m_p - m_{\bar{p}}| < 0.5$ MeV), a relative precision of 5×10^{-4}, which has of course been superseded by direct measurements on trapped antiprotons.

Relatively low resolution fluorescence spectroscopy of the X-ray transitions at the end of the antiatomic cascade provided valuable information on the strong interaction or permitted identifying the last state reached in the cascade, and from which annihilation occurs (allowing mapping the nuclear density distribution, see Section 5.4.4).

The sensitivity of such early measurements of antiprotonic He at CERN's PS [144] was not sufficient to detect the small fraction of long-lived ($\sim \mu$s) meta-stable states discovered in 1991 [117]. These states opened the door to high precision laser-spectroscopic studies of the energy levels of the antiprotonic atoms by the PS205 (at LEAR, until 1996 [145]) and the ASACUSA (at the AD) experiments, see Section 4. This methodological advance over resolution-limited X-ray detectors consequently improved the knowledge of the mass, charge and magnetic moment of the antiproton by many orders of magnitude beyond what measurements of the de-excitation cascade could provide.

Revisiting these questions, which were well explored within the detectors' technical limits until the replacement of the continuous antiproton beam of LEAR with the pulsed extraction of CERN's Antiproton Decelerator, requires novel approaches to the formation of antiprotonic atoms.

5.2. Formation and evolution of antiprotonic atoms

Formation of antiprotonic atoms was studied in detail by Cohen in the context of capture of negative particles by atoms, ions and molecules [142]. With the exception of the charge exchange processes used to form antihydrogen, the specific processes of capture at the atomic level are similar for all experimental realizations to date, which consist of injecting low-energy antiprotons into a target material (ranging from solid to liquid to dilute, cold gas); the required slowing down

of antiprotons in sufficiently dense media prior to capture and the initial stages of the capture process (with unobservable Auger emission and low-energy cascade photons, none of which escaped the dense targets) could not experimentally be observed. Furthermore, at realistically achievable densities in this approach, interactions between the antiprotonic atoms and other atoms of the medium lead to density-dependent de-excitation processes, and consequently annihilation from a wide spectrum of initial quantum numbers.

Going beyond this experimental limitation requires new approaches to formation of antiprotonic atoms which build on trapped antiprotons and trapped atoms, ions or molecules; the corresponding formation techniques will be discussed below. Independent of the specific formation scheme however, the physics involved in replacing an electron by an antiproton remains the same.

As in the case of formation of antihydrogen, both three-body recombination processes and charge exchange processes can be used to form antiprotonic atoms or atomic ions (in the former case) or antiprotonic atoms (in the later). In the former case, injection of (negative) antiprotons into (positive) atomic (or molecular) ions trapped in a nested Penning trap configuration leads to quasi continuous formation of antiprotonic atomic ions over time scales of seconds (Fig. 3, right). For these processes, simultaneous laser cooling of the positive ions is imaginable, thus ensuring the formation of relatively low energy Rydberg atomic ions, whose lifetime is however likely to be very short (even in antiprotonic He, the vast majority of annihilations occur on timescales of ns after formation of the antiprotonic atom), thus ensuring that the annihilation process occurs within the immediate vicinity of the point of formation, within the Penning trap for positive ions.

While an analogous formation process to that of three-body recombination (Eq. (1)) is envisagable:

$$A^+ + A^+ + \bar{p} \rightarrow \bar{p}A^* + A^{+'} \tag{6}$$

and results in the formation of neutral antiprotonic **atoms**, the reaction rate is low in comparison to the dominant three-body recombination process [14]:

$$A^+ + \bar{p} \rightarrow \bar{p}A^{++*} + e^- \tag{7}$$

where the role of the third partner of the three-body recombination is played by one of the remaining electrons of the partially ionized ion A^+ and which forms antiprotonic **ions**. The corresponding $\bar{p}$-energy dependent capture cross sections of up to 10^2 (in units of a_0^2) are very similar to those of the atomic capture cross section [24], although in the case of He^+ (with a single remaining bound electron), a quantum-mechanical study [146] results in a more complex picture, with relatively strong suppression of the antiproton capture rate in the ionic, with respect to the atomic, system. In both models however, an important feature is that the capture cross section increases strongly with decreasing relative energy, thus emphasizing the importance of working with low temperature atomic ion and antiprotonic plasmas.

The situation is different in the case of charge exchange: here, *negative* ions co-trapped with antiprotons are a suitable starting point. Charge transfer reactions between ions and Rydberg atoms result in Rydberg atoms with principal quantum numbers similar to that of the original Rydberg atom [147]). The formation process proposed for antiprotonic Rydberg atoms is a pulsed-laser controlled process, with several laser pulses firing within a few ns of each other. The first step is to photo-ionize the anionic species; immediately thereafter, several further laser pulses excite the now neutral species from its ground state A_g into a Rydberg state A_n^* via an intermediate state A_e are possible. While direct excitation from the ground state is also feasible in principle, lasers at the requisite wavelengths are daunting. Whether starting from a ground state system or from a Rydberg system, the resulting charge exchange between the neutral system and the antiproton results in the formation of a Rydberg antiprotonic system; it is only the principal quantum number n' of the formed system that will be changed:

$$A^- + \gamma_1 \rightarrow A_g + e^- \tag{8}$$

$$A_g + \gamma_2 \rightarrow A_e \tag{9}$$

$$A_e + \gamma_3 \rightarrow A_n^* \tag{10}$$

$$A_n^* + \bar{p} \rightarrow \bar{p}A_{n'}^* + e^- \tag{11}$$

In the case of e.g. ground state H, the resulting $\bar{p}$H will be in $n' \sim 40$; in the case of H(n=30), the resulting $\bar{p}p^*$ will be in $n' \sim 2000$ [94], with an angular momentum distribution enhanced towards the circular $l \sim n'$ states. Consequently, lifetimes well in excess of 10's of μs can be obtained for the Rydberg states, although if no prior excitation of the initial atom is undertaken, then those timescales shrink to ns.

In the absence of the possibility (for now, although there are ongoing attempts [148]) to laser-cool the anionic species, the final temperature of the resulting antiprotonic atoms will be determined by the equilibrium temperature of the anions achieved through sympathetic cooling via co-trapped electrons, typically in the region of 10's of K. In both trap-based formation processes, the local density of atoms is such that, in contrast to formation in gaseous, liquid or solid targets, interactions between surrounding atoms and antiprotonic atoms is negligible, so that the atoms evolve as isolated systems and, after an initial phase possibly including Auger electron emission, rapidly reach circular Rydberg states $(n, l = n - 1)$ [149]. In $Z > 2$ Rydberg atoms, and neglecting the influence of external fields, only collisional Stark mixing of states $(n, l \rightarrow n, l')$ in collisions between Rydberg atoms and any possibly present ions [150,151] could

potentially influence the evolution of the system; in the chosen trap-based scenario, this is negligible, as are collisional n and l changing collisions with surrounding ground state atoms [152]. The subsequent cascade (Section 5.4.3) will result in a step-by-step ejection of more deeply bound electrons, albeit at a slower rate, leading to either fully stripped atoms or atoms with only the most deeply bound electrons remaining at the moment at which annihilation of the deeply bound antiproton with the nucleus takes place. In this temporal evolution, the antiprotonic atoms pass through a number of regimes that each have a specific physics interest, and which can be probed by an appropriate choice of formation mechanism, resp. choice of formation parameters.

Laser manipulations, spectroscopy and study of interactions between formed antiprotonic Rydberg atoms require long-lived states for which, furthermore, the time of formation is known, so as to be able to e.g. manipulate or probe them with further laser or microwave fields. On the contrary, nuclear processes that occur at the end of the cascade may be better studied via three-body formation processes or charge exchange formation processes without a prior excitation of the atom, which ensures that annihilation between antiprotons and protons or neutrons takes place within the same potential well as that within which the antiprotonic atoms were formed. In an alternative approach, that of prior Rydberg excitation of the target atom, nuclear interactions between the antiproton and the nucleus will occur far away from the formation Penning trap that furthermore will only trap *negative* ions.

If no Rydberg excitation is thus carried out, then annihilation of the antiproton with the nucleus will occur on timescales of ns after capture. Naturally, given the fact that the moment of neutralization of the anion is known to O(10 ns), and thus that of the subsequent formation of the antiprotonic atom in a plasma with radius of 100 μm to O(1 μs) accuracy, switching the polarity of the trap so that only positive ions remain trapped, or working within a nested Penning trap, would allow trapping any formed highly charged nuclear remnant or fragments, as long as their recoil energies remain lower than O(1 keV), which corresponds to annihilations between antiprotons and very peripheral nucleons. This is discussed in detail in Section 5.4.5.

Similarly, performing a more complex sequence of steps on co-trapped A^-, H^- and $\bar{p}$ would allow not only forming (possibly trappable) nuclear remnants, but would also allow exposing them (only 10's of ns after their formation) to Rydberg protonium, initiating a further charge exchange process, and forming (hollow) Rydberg atomic ions consisting of the nuclear remnant or nuclear fragment and the antiproton very briefly after their formation. These hollow Rydberg atomic ions can then be studied spectroscopically (see Section 6.1).

5.3. Antiprotonic Lithium

Before focusing on antiprotonic atoms of heavier nuclei, a short discussion of the special case of antiprotonic lithium is in order here. As noted above, a small fraction of antiprotonic He atoms end up in metastable states, with lifetimes of the order of μs. Annihilation is suppressed by the difficulty of Auger ejection of the remnant electron in the case where $l \sim n$ [153] since the Auger transition requires a large angular momentum change. Several authors have investigated not only this special case, but have also attempted to investigate whether similarly long-lived states of $\bar{p}Li^+$, of $\bar{p}Li^{++}$ or of the anionic $(\bar{p}e^-e^-\alpha)$ systems might also exist. From a calculation for circular and almost circular states [154], it appears that in addition to $\bar{p}$He, for specific values of l, also long-lived (O(μs)) states of $(\bar{p}e^-e^-Li)$ should exist. More recent semi-quantitative [155] or semi-classical calculations [156] have bolstered the expectation that some $\bar{p}$Li atoms should be sufficiently stable against Auger decays to be observable as long-lived states; specifically, $\bar{p}Li^+$ with $l \leq 30$ can have large Auger decay rates, while states with $l \geq 40$ should be long-lived, with states with $l \geq 50$ having practically negligible Auger transitions. Spectroscopy of such states would then expand the systems in which very high precision spectroscopy of simple antiprotonic atoms could be carried out, allowing an independent evaluation of the systematic errors of spectroscopy of the $\bar{p}$He system.

Obtaining such high angular momentum states in interactions between antiprotons and Li atoms is however challenging, since replacement of the outermost electron will lead to $n \sim 40$ antiprotonic Li atoms, with an l-state distribution that also has significant population at low l values and which furthermore will undergo, even in a dilute gaseous environment, collisional de-excitation. Indeed, experimental searches for meta-stable antiprotonic Li have been unsuccessful: only a handful of experiments have attempted to search for long-lived $\bar{p}$Li states in the decay spectrum of antiprotons injected into (solid) Li, the most sensitive one finding that at most, 0.015% of antiprotons are trapped into long-lived states [157].

The key to forming potentially long-lived $\bar{p}$Li states thus lies in reaching the $l \sim n$ states with sufficiently high l that Auger transitions are highly unlikely; if the initially formed antiprotonic atom is in a sufficiently excited state $n_{Rydberg}$ at the moment of formation (as can be achieved via the pulsed formation scheme with intermediate Rydberg excitation of the atom described in Section 5.2), then the antiprotonic atom can radiatively reach such a meta-stable high-l circular or near-circular state. At the same time, however, such *neutral* antiprotonic atoms are not contained within the formation Penning trap, and instead will reach the trap electrode surfaces (and annihilate) on timescales of O(100 μs) for $T \sim 10$ K Li (and correspondingly longer for heavier atoms), thus requiring either a multipolar magnetic trap for temporary trapping or starting with Li excited into low-lying states (which thus can decay with time constants of μs).

5.4. Antiprotonic atoms beyond Li

Antiprotonic helium (both ^{3}He and ^{4}He) has become a high precision laboratory for the determination of the mass and charge of antiprotons due to its particularly long-lived metastable states (with lifetimes of the order of 10 μs) that allow complex manipulations with optical and microwave radiation. Other antiprotonic atoms are however short-lived, in spite of being initially formed in Rydberg states; de-excitation occurs via cascades of Auger processes and only where these are not possible, via radiative transitions. In helium, such Auger transitions are suppressed, at least in the case where the $\bar{p}\mathrm{He}^+$ atoms have large principal quantum number n and an angular momentum number l close to the maximal value of $n-1$. The low likelihood of large angular momentum changes between such near-circular states required to Auger-eject the second electron and that would result in rapid de-excitation and annihilation leads to the long lifetimes of these intermediate states.

Experimentally, such large n, l values do not appear in the formation of other antiprotonic atoms, which may however partly be due to the manner in which they are formed, and partly to the environment in which they are formed (high density, and thus elevated likelihood of multiple interactions with other atoms). As indicated above in Section 5.2, these limitations might be overcome by forming antiprotonic atoms (and molecules) in a very low density environment, in which they can essentially be treated as isolated systems, and may thus – if starting from very high excitation levels – slowly de-excite radiatively to reach the $l = n - 1$ diagonal.

Studies of antiprotonic atoms can be separated into two domains: the first concerns spectroscopy of transitions between Rydberg levels, with frequencies in or close to the optical regime which can, e.g. in the case of $\bar{p}$He, be stimulated via lasers or microwaves. The second concerns transitions between deeply bound states of heavy atoms, with transition energies in the keV region, and thus observable only via detection of the fluorescence photons. While in the later case, strong interaction shifts of the most deeply bound state reached before annihilation are particularly interesting (but for which measurements are unfortunately limited not only by available statistics and by the model used to extract the shifts, but also by the resolution of the detectors for the keV photons), precision measurements of transitions between the excited levels (potentially via laser or microwave spectroscopy) are particularly sensitive probes of the properties of antiprotons, of QED, and of the presence of non-standard model interactions.

To date, only in $\bar{p}$He has it been possible to study and measure transitions between Rydberg states, first by single-photon-induced transitions, and subsequently by two-photon spectroscopy. To minimize Doppler broadening of those transitions, two-photon spectroscopy of $(n, l) \rightarrow (n-2, l-2)$ transitions are particularly suited, with the caveat that the large mass of the antiproton results in small probabilities for these non-linear transitions, and that fine tuning of the intermediate virtual state close to the $(n-1, l-1)$ level is required to achieve the necessary rates [158]. The extremely short lifetimes of other antiprotonic atoms has excluded such studies to date; the formation of highly excited ($n \gg 40$) antiprotonic atoms via production in traps however opens the possibility of studying non-$\bar{p}$-He systems as well. In light of the very high precision achieved in $\bar{p}$He, it is however important to consider which systems it might be worthwhile to attempt spectroscopy in, and which physics topics could be addressed that have not yet been covered. The following sections will address these specific areas that deal with QED tests and searches for beyond-standard-model physics; the potential of producing spin-polarized antiprotons; and the study of nuclear physics made possible by forming antiprotonic Rydberg atoms. A discussion of the specific case of highly charged hollow Rydberg atomic ions can be found in Section 6.1.

The following two sections discuss first the highly excited Rydberg states and transitions within them, before focusing on studies of the deeply bound states.

5.4.1. Antiprotonic Rydberg atoms and tests of QED

Transitions between Rydberg states are sensitive to the presence of physics beyond the standard model (in the form of e.g. light scalar models or chameleons [159]), or forces mediated via kinetic mixing between a photon and a new Z' [160] which would result in modification to the standard model interaction strength between the nucleus and electrons. Calculations for a wide range of transitions in hydrogen [161] indicate that the sensitivity is limited on one hand by the much greater uncertainty of Rydberg levels with respect to the precision of the $1s-2s$ transition (which is known to the 0.01 ppt level in H), and on the other hand, by the very limited number of (n, l) states for which precise data exist. A measurement of a large number of Rydberg transitions to a comparable level of precision as that of the $1s-2s$ transition has the potential to improve existing limits on the electron–mediator coupling by several orders of magnitude over a very wide range of mediator masses (between 1eV and 10 keV).

The same holds for exotic atoms, among them antiprotonic Rydberg atoms, which are a novel testing ground for high-field bound-state QED [1], which is traditionally probed with mostly or fully stripped ions, typically in accelerator facilities, where these few-electron high-Z ions are spectroscopically probed in flight. Experimental uncertainties are at the 10 or even 100 ppm level, and even potentially more precise measurements of the lowest-lying levels in such 1-electron atoms will remain affected by finite nuclear size and nuclear polarization effects. Antiprotons captured by (singly charged) trapped cations (in two-body, and considerably more rarely in three-body, interactions) or by ground-state atoms (in charge-exchange reactions) are directly trapped into low-lying *atomic* states, which however correspond to Rydberg states for the antiprotons; for light and medium-Z atoms, all electrons are Auger-ejected, while for high-Z atoms, a small fraction of the (deepest-bound) electrons remains [149,162], while the antiproton is still in a highly excited state.

In particular for high *n circular* states, nuclear contributions are negligible, while bound-state quantum electrodynamics contributions remain large. The type of spectroscopy of the intermediate level transitions in these antiprotonic atoms will

depend on the atomic levels being observed. For lower-lying states, fluorescence spectroscopy should be able to probe down to energy resolutions of better than 1 eV [163]. Both for the neutral (and thus untrapped) antiprotonic atoms, as well as for the completely stripped (with the exception of the antiproton) atomic ion, the energies of the transitions between the more deeply bound states are in the range of 10's to 100's of keV. Probing transitions among more highly excited Rydberg states requires the more complex, but most likely still feasible multi-step approach delineated in Section 5.2 (for formation) and 5.4.3 (for exciting transitions within Rydberg states). This which would however have an enormous advantage over fluorescence detection, since those transitions could not only be laser-stimulated, with a concomitant much higher precision, but could also take place with charged, and thus trapped, systems. As pointed out in [1], probing second-order QED effects across a wide range of Z becomes possible in such systems, and thus, the structure of the vacuum can be tested in configurations in which the Schwinger limit is largely exceeded by the average field strength.

5.4.2. Antiprotonic Rydberg atoms as a path towards polarized antiprotons?

Obtaining polarized antiprotons has long been a goal for a number of subsequent measurements (measurements of scattering cross sections of polarized antiprotons, disentangling of contributing partial waves in the formation of hadronic states via control of the spin configurations in antiproton–proton annihilations) and a number of attempts have been made to search for polarization effects that would lead to such a beam [164–168]. Any polarizations resulting from spin-dependent interactions or spin build-up in accelerators have unfortunately turned out to be very low.

However, one interesting approach with much higher potential polarization has been suggested by K. Imai [169] and relies on the intermediary formation of antihydrogen atoms: in his proposal, antihydrogen atoms are formed in co-circulating positron and antiproton beam, and are subsequently optically pumped via circularly polarized light over a 10 m long flight distance. Production of antihydrogen atoms in nested traps results in production rates of antihydrogen of $10^3 \sim 10^4$ $\bar{H}$/s, albeit into 4π and in a range of Rydberg states, while the above scheme requires ground state atoms, and was thus not immediately applicable. With the advent of trapped antihydrogen, however, and the microwave manipulation of the trapped species (Section 2.3), antiproton-spin selective depopulation of the trapped ensemble becomes feasible, albeit currently resulting in low numbers of potentially spin-polarized antiprotons (with respect to the axial Penning trap magnetic field).

An alternative approach might potentially be provided by antiprotonic atoms and molecules: antiprotonic atoms formed via resonant charge exchange in Penning traps will be in highly excited but relatively well-defined $l \sim n$ Rydberg states, and will form a relatively dense cloud for 10's of μs after their (pulsed) production, during which time they can be manipulated (as can be atoms of antiprotonic Helium formed more conventionally, and for which antiproton-spin selective transitions have already been induced via microwaves — see Section 4). The target atom or ion itself is furthermore amenable to manipulation prior to formation of the antiprotonic atom: polarization of the lasers involved in the excitation process into a Rydberg state allows influencing the magnetic substate m of the resulting Rydberg atom [170].

During the relatively long drift time as the cloud of any formed antiprotonic Rydberg atoms expands, spin-selective processes, e.g. microwave-induced transitions or circularly-polarized optical pumping of antiprotonic Rydberg atoms of paramagnetic elements, like Rb [171,172], could preferentially depopulate particular antiproton spin orientations with respect to the Penning trap's axial magnetic field. Alternatively, a (radial) magnetic gradient field superimposed on the Penning trap would act differentially on different spin states, selectively accelerating outwards one orientation, while decelerating the other, although this approach is more challenging for Rydberg atoms in a wide range of internal states.

Finally, embedding antiprotons into molecules (first forming Rydberg molecules, analogously to the formation of Rydberg target atoms prior to forming antiprotonic Rydberg atoms) opens a further possibility: spin-polarized hydrogen can efficiently be obtained from the photolysis (using circularly polarized light) of a simple di-atomic molecule, e.g. HCl [173], in which polarizations of 36% are obtained.

Ultimately, photo-ionization of the polarized antiprotonic bound systems will then be required to produce an ensemble of polarized antiprotons within the formation trap's magnetic field, which will then need to be extracted for subsequent measurements. Among these, one could be particularly interesting, as it would allow a novel test of CPT within the same device as for protons: recently [174], a proposal has been made to build a custom electrostatic storage ring to search for a permanent electric dipole moment of the proton (pEDM). The aimed-for sensitivity of 10^{-29} e·cm is achieved by using polarized "magic" momentum 0.7 GeV/c protons in an all-electric storage ring. The same storage ring structure would work equally well for polarized antiprotons of the same momentum, furthermore allowing reducing systematic errors (remnant E-fields), which would require developing techniques for antiproton polarimetry, but would permit searching for a putative $\bar{p}$EDM in parallel to the pEDM.

5.4.3. Atomic cascade in antiprotonic atoms

Initial investigations of the transitions of antiprotonic atoms focused on the transitions between the most deeply bound states, with transition energies in the keV $\sim$ 100 keV range, as a way to investigate on one hand cascade models and the dynamics of the depletion of electron shells, and on the other hand the $\bar{N}$N potential through strong interaction shifts and broadenings of the most deeply bound states. As an example of the former, in the case of the noble gases Ar, Kr and Xe, the principal quantum numbers of the outermost electron shell are $n_e = 3$, 4 and 5, resulting in initial $n_{\bar{p}}$ of the corresponding antiprotonic atoms of 128, 170 and 215, thus allowing in principle following a very large number of de-excitation steps. In a detailed study of antiprotonic atoms of noble gases [149], the relative intensities of the different transitions, the presence and energy distributions of electronic L- and K-X-rays, and comparison with a calculation of electronic and antiprotonic binding energies in a multi-configuration Dirac–Fock (MCDF) approximation that includes radiative and nuclear finite size corrections [175] allowed extracting a number of central features of the cascade in these noble gases:

- in dilute gases, refilling of Auger-ejected electrons from neighboring atoms or molecules is very strongly suppressed;
- in the course of the cascade, the binding energy of the remaining electrons increases due the reduced screening of the nuclear charge, which can effectively temporarily interrupt the Auger de-excitation; such levels should be meta-stable (only radiative transitions can take place to lower levels) and might thus be amenable to laser-assisted transitions into other, less stable levels;
- complete ionization is reached in lighter systems (krypton), while not in heavier ones (xenon). In this later system, once the antiproton has reached the $n_{\bar{p}} = 22$ level (52-fold ionized Xe), while almost all electrons will have been ejected, L-shell depletion must be considered to remain incomplete. The binding energies of the remaining two K-electrons are 40 271 and 41 300 eV. These energies are reduced to 38 793 and 39 028 eV if the antiproton screens one of the two charges, and a transition from $n_{\bar{p}}$=16 to 15 (Δ(E)=39 028 eV) is enough to eject one K electron (but only if the other is still present). Subsequent transition energies are $\bar{p}$Xe(15-14): 47 708 eV and $\bar{p}$Xe(14-13): 59 167 eV;
- resolving a number of electronic X-rays requires a major technological step forward over semiconductor detectors (with an energy resolution of ∼1%), which would also open the possibility of Auger electron spectroscopy of the de-excitation cascade in very low density environments that exclude refilling of any Auger ejected electron levels. X-ray detectors with the requisite sub-‰ energy resolution are slowly coming within range [163].

Contrary to the early spectroscopic measurements that relied on a beam of continuously extracted antiprotons for tagging the start of a capture and cascade sequence, and possibly, as in the case of antiprotonic helium, inducing level changes from metastable to short lived states, forming antiprotonic atoms in traps offers a wider degree of freedom. This concerns particularly the case of initially highly excited Rydberg atoms, as these will to a very large extent reach the $l = n - 1$ states early on, and undergo (slow) radiative transitions instead of the rapid de-excitation process of Auger transitions. These Rydberg atoms can be temporarily trapped (on time scales commensurate with the radiative transition times) in a magnetic gradient trap as they undergo radiative transitions (although evaluating the trappability of specific high-n, high-m Rydberg atoms is complex [176,177], the required magnetic field gradient should be significantly smaller than that required to trap ground state antihydrogen). Furthermore, also a much larger fraction of formed antiprotonic atoms than the $\sim$ 3% in the case of antiprotonic helium would be susceptible to be affected by level-changing laser pulses, thus allowing a much more high-resolution investigation of the early steps of the cascade. Additionally, replenishing of any Auger-ejected electrons should be negligible in comparison to already low levels in previously-used dilute gas targets.

Similarly to frequency scans across a resonance in antiprotonic helium, which induce transitions between metastable and short-lived states, resulting in a laser-frequency dependent annihilation signal, a method to de-excite or ionize meta-stable antiprotonic Rydberg atoms is required, with the understanding that any formed Rydberg atoms will be spread across a large number of (n, l) states, and that subsequent Auger de-excitation can occur only once n$\sim$ 40 is achieved. De-excitation of Rydberg states is a non-trivial undertaking [178]. One way to carry out such Rydberg spectroscopy has been proposed by Hayano [114], and builds on detecting lifetime differences between resonantly-populated longer-lived Rydberg levels with respect to shorter lived initial Rydberg levels; another possibility could be resonant photo-ionization and subsequent detection of the liberated $\bar{p}$ in the case of in-flight spectroscopy.

5.4.4. Nuclear halo

Even more deeply bound states are however beyond the domain accessible even via XUV lasers; here, fluorescence spectroscopy of the occurring transitions allows measuring transitions and their widths to better than 0.1% (with superconducting microcalorimeters [163]) or, in the case of dedicated Bragg spectrometers [11], even to $\sim 10^{-4}$. Over the course of several decades, antiprotonic atoms of a large number of elements have been measured and analyzed in terms of the interaction potential between the nuclei and the antiprotons, respectively the optical model that is built on it. Recent considerations on the properties and problems arising from such an ansatz, and discussing antinucleon–nucleus interactions in the framework of the optical potential, can be found in [179–181]. Nuclear absorption reduces the lifetime of the lowest accessible atomic state, resulting in a broadening of this X-ray line, while the strong interaction itself shifts the energy of the last level reached by the antiprotonic atom from its purely electromagnetic value. As the strong interaction potential is proportional to the nuclear matter density, the widths and shifts provide information on the nuclear density at the point of annihilation (the last available level or the last-but-one level). Note that X-rays are produced not only during the (rapid) cascade, but also through the acceleration of charge at the moment of annihilation. This inner bremsstrahlung continuum [102] can furthermore interfere with the transition lines, on one hand potentially yielding additional information, but on the other distorting the measured spectra. This effect has not been taken into account in systems other than protonium. A number of studies focused on isotopes of Mo [182], Nd [183], Te, Sm and Pt [184], O [185], Li [186] or of Yb and Ba [187], in addition to a number of further elements. The PS209 experiment at LEAR in particular determined a large number of level shifts (44) and level widths (62) for 34 different isotopes [188], whose analysis is summarized by Fig. 11.

These studies of antiprotonic atoms, both of their fluorescence cascade and of the distribution of nuclear fragments resulting from the annihilation of antiprotons with the nucleus (via radiochemical methods), has allowed extracting information about the nuclear periphery of specific atoms, albeit on a statistical basis. Furthermore, it should be pointed out that the neutron density distribution is more difficult to measure accurately than the proton density distribution

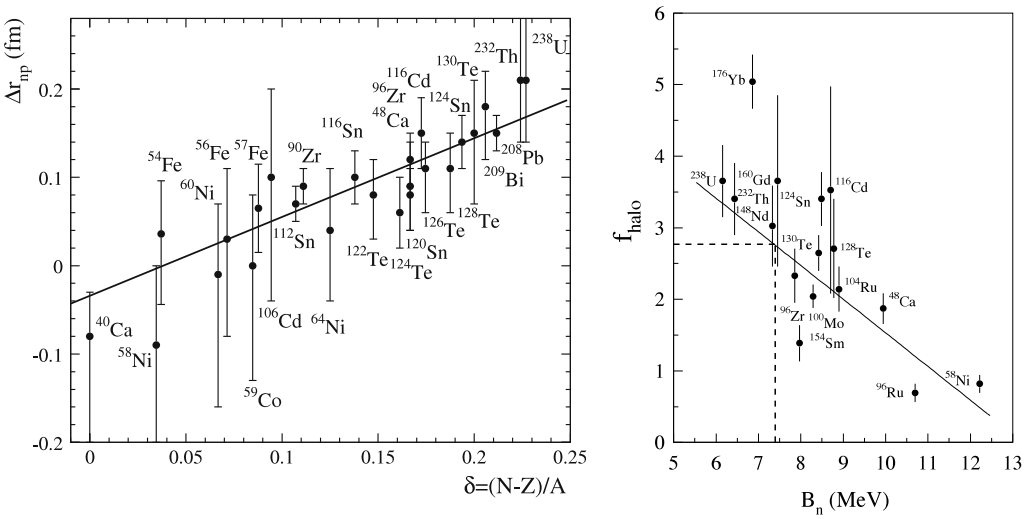

Fig. 11. Left: Difference between the rms radii of the neutron and proton distributions, deduced from antiprotonic X-ray data, as a function of $\delta = (N-Z)/A$. Right: A straight line fit to the experimentally determined [189–191] halo factors (see [192] for a definition), plotted as a function of the target-nucleus neutron binding energy. For ^{208}Pb, the neutron binding energy is equal to 7.4 MeV and the interpolated halo factor is 2.8 ± 0.4. *Source:* Reproduced from [188,192] with permission.

(which can be probed by non-strongly interacting probes, such as electrons) because it interacts mainly with hadronic probes (protons, alphas, pions and antiprotons) through non-perturbative interactions whose theoretical description is model dependent. The neutron skin of 26 antiprotonic atoms ranging from ^{40}Ca to ^{238}U was systematically analyzed by the PS209 experiment [188]; under the assumption that the neutron and proton densities at large radii are well described by a two-parameter Fermi distribution, the authors conclude that for neutron rich nuclei it is mostly the neutron diffuseness which increases and not the half-density radius. This outcome suggests that there is a correlation between the neutron skin thickness and the isospin asymmetry, and that the concept of neutron "skin" (in contrast to neutron "halo") is not necessarily the best description of the data, although this conclusion rests to some extent on the details of the modelization [193,194].

While the uncertainties stemming from experiments with antiprotonic atoms are larger than other approaches (electron scattering, …), reduced experimental (and theoretical) uncertainties over a range of further isotopes would allow an improved determination of the skin thickness of e.g. the particularly interesting stable nucleus ^{208}Pb [195,196]. This nucleus has already been the target of spectroscopic observations: a measurement of the fine-structure splitting in the circular 11→ 10 X-ray transition of $\bar{p}^{208}$Pb [197] allowed determining the magnetic moment of the antiproton at the ‰ level. In addition to revisiting and expanding on these measurements, further specific isotopes are also worthy of further detailed study, such as deformed even-A nuclei (search for an LS effect), odd-A nuclei (influence of an unpaired nucleon on the density distribution), or doubly magic Ca isotopes.

Radiochemical methods to characterize the type of annihilation ($\bar{p}$p vs. $\bar{p}$n) are mainly sensitive to radioactive annihilation fragments; any long-lived or stable remnants naturally remain invisible. Forming antiprotonic atoms in traps opens up the possibility of event-by-event determination of the emitted fluorescence X-rays together with the determination of the charge multiplicity of the annihilation, allowing to disambiguate antiproton annihilations on protons (total charge = 0) from those on neutrons (total charge = -1), as long as all mesons resulting from the annihilation are detected. In addition, as these experiments would take place in vacuum, there is the possibility of detecting and characterizing even the formed nuclear remnants, whether they are stable or not. Earlier experiments at LEAR with streamer chambers were already sensitive to such nuclear fragments, measuring their (undifferentiated) momentum distribution for $\bar{p}^4$He and $\bar{p}$Ne [198,199], but also extracting the relative $\bar{p}$n and $\bar{p}$p annihilation strengths, from which a degree of inconsistency between the halo and the low-Z measurements emerges. Such studies can furthermore be extended to unstable nuclei, for whom characterization of the nuclear periphery is particularly interesting, specifically for very neutron- or proton-rich isotopes.

The PUMA experiment [3] thus has the goal of forming antiprotonic atoms of short-lived radio-isotopes in order to probe, through antiproton–neutron and antiproton–proton annihilation, the long distance tail of the nuclear potential for unstable nuclei; this requires combining a (transportable) trap for antiprotons with a tracking detector for the annihilation products. As for the stable isotopes, this allows investigation of the neutron skins of proton- or neutron-rich isotopes, and thus better characterizing the neutron density distribution in the halo of nuclei (and thus the nuclear symmetry energy [200]). It has to be pointed out that using hadronic probes such as antiprotons results in rather large systematic uncertainties, since in hadronic processes the probe and the target are inextricably linked, so that a 'truly

model-independent determination of the density distributions is impossible' [201]. Nonetheless, a range of approaches (relativistic mean field, optical potential) to calculate the $\bar{p}$ binding energies and level widths give consistent values of the 1s state for a range of nuclei [202]. This not only strengthens confidence in the specific form of the used $\bar{p}$ optical potential near threshold and in a low nuclear density region, of relevance for determination of the precise functional form of the neutron density distribution, but furthermore constrains extrapolations to higher densities into the sub-threshold region and thus to the region relevant to potential $\bar{p}$-nuclear bound states. Indeed, calculations indicate that if an antiproton is embedded in the nucleus, the later is compressed and the nuclear core density increases, reaching a value 3-4 times the normal nuclear density in the vicinity of the $\bar{p}$ [203]. Such antiproton–nucleon or antiproton–nucleus quasi-bound states (lifetimes would be of the order of 10^{-23}s) have been searched for at the LEAR facility at CERN and at BES [204]. While those attempts have been unsuccessful or inconclusive, more recent calculations (such as chiral effective theories in [205]) continue to maintain interest in the possibility of observing these putative states.

5.4.5. Annihilation with protons and neutrons: fragmentation

Antiprotonic atoms $\bar{p}$A have cascade times on the order of ns [142], so that a few ns after the atom is formed, annihilation of the antiproton with a peripheral neutron or a proton of the nucleus occurs, initially leading to ${}^{Z}_{N-1}A$ or ${}^{Z-1}_{N-1}A$ together with any mesons (mainly pions, but occasionally also kaons) produced in the $\bar{p}$-nucleon annihilation. Secondary interactions between the nucleus and these mesons have been studied both experimentally and theoretically. Models based on intranuclear cascade models [206] or on a microscopic transport approach [207], as well as many others, reproduce the global structures of the experimental data that have been collected for antiproton annihilations on e.g. Au [208], Mo or Ho [209]. The models themselves proceed by steps: after the annihilation of the antiproton with a nucleon, any produced pions (or kaons) that travel through the nucleus deposit energy and initiate a cascade process in which some nucleons can be ejected with high energies, while the remaining nuclear remnant de-excites further via evaporation. An overview of many aspects of the field can be found in [210].

It has to be pointed out that, given experimental limitations, only the lightest fragments resulting from annihilations of antiprotons on nuclei have been investigated with direct detection of those fragments [211], but without the possibility of measuring their energies, or their undifferentiated momentum distribution [198,199]. For heavier fragments, only bulk mass spectrometry of a large number of antiproton–nucleus annihilations has been carried out, generally via radiochemistry (which is naturally insensitive to long-lived or stable nuclear fragments).

Both from the models and from experimental data (e.g. from antiprotons annihilating on Au), two structures emerge: on one hand, it has become clear that the $\Delta N = -1$ process, i.e. in which the remnant nucleus is only slightly disturbed, losing either a proton or a neutron but otherwise receiving only enough energy to allow γ-transitions, but not enough to eject any nucleons or nuclear fragments, is very common, occurring in 10% ∼20% of the cases, even for heavy/large nuclei such as Pb, as is shown in Fig. 12. The prevalence of this $\Delta N = -1$ process indicates that peripheral, low momentum transfer annihilation is common, an observation that is crucial in studies of the nuclear periphery detailed in Section 5.4.4. Furthermore, processes in which A or Z are reduced by one unit (corresponding to peripheral antiproton–neutron or antiproton–proton annihilation with an otherwise unperturbed nucleus) are clearly competitive with more disruptive processes resulting in production of nuclear fragments or boil-off of nucleons.

While for peripheral annihilations, only little recoil energy is transferred to the remnant nucleus (see following section for a discussion), for more energy deposited in the nucleus, the result is a broad range of possible nuclear fragments, whose detailed ratios are broadly described by the different theoretical approaches, and where yields are very broadly clustered around 45% and 85% of the mass of the parent nucleus, with the lower region corresponding to fission products, and the higher region to evaporation residues. In the specific case of antiprotons annihilating on gold, the fission yield is (3.8 ± 0.5 %) [208]. The quantum molecular-dynamics model (the LQMD transport model, [207]) that combines the production of primary fragments via a coalescence approach, as well as their subsequent decay via evaporation of nucleons (via the statistical code GEMINI), reproduces particularly well the available data on fragment production from LEAR at CERN. Although beyond the scope of this review, it is worth mentioning that the formation of hypernuclei (through the interaction of kaons produced in the annihilation reaction with the primary precursor nucleus), or more precisely, of hyperfragments [214] is also well described by the same model. Hyperon production in $\bar{p}$-N interactions is a sensitive probe for the properties of the antikaon–nucleon interaction in the nuclear medium, with implications also for the study of the appearance of deconfinement [215].

5.4.6. Formation of trapped highly charged ions (HCI's)

As indicated in Section 5.4.3, shortly before the antiproton in an antiprotonic atom reaches the nuclear periphery (in fact, once its wave function is within that of the innermost electron) and annihilates, the atom is fully stripped (or almost fully, in the case of nuclei heavier than Kr, albeit increasingly less so with higher A, as the deepest-bound electrons are then not Auger-ejected). The resulting system consists of the nucleus, the remnant antiprotonic ''heavy electron'', and possibly a small number of very deeply bound electrons. Experiments with a range of antiprotonic atoms showed that in 10∼20% of the annihilations, the nucleus remained intact [206]. If this process takes place in a nested trap configuration (injection of antiprotons into trapped positive ions), the resulting (highly positively charged) daughter nucleus will experience the strong (due to its Z-fold nuclear charge) electric field of the Penning trap in which it was formed. But also pulsed formation can result in the same situation, either by embedding the well holding the anions and the antiprotons within

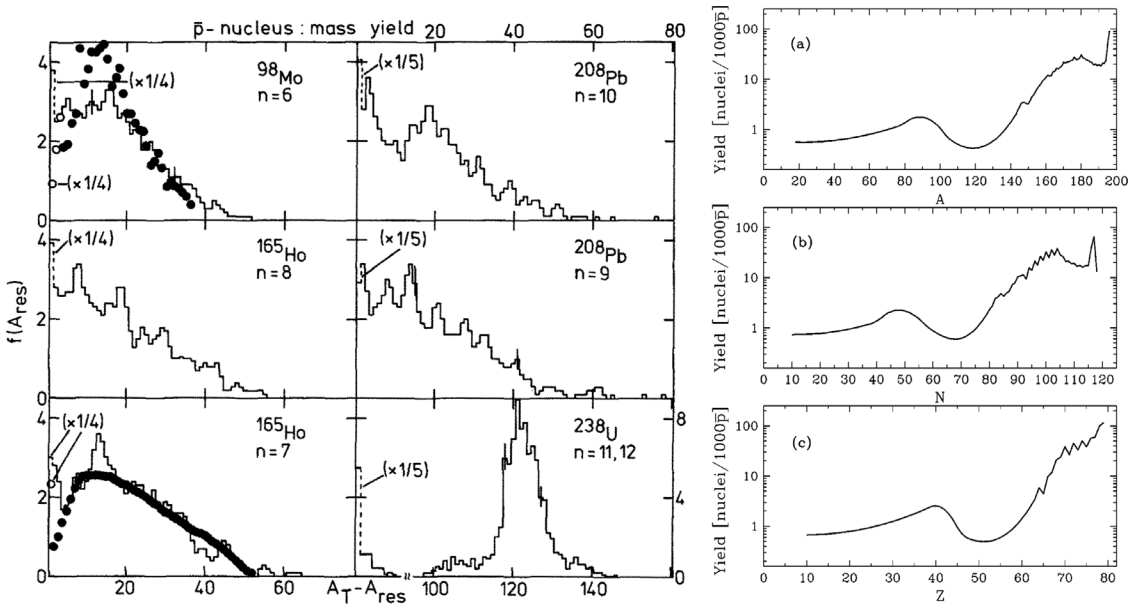

Fig. 12. Left: Probability distribution (in percent) for the residual mass A_{res}. The histograms are the results of the model in [206]. The dots and the open circles are data on ^{98}Mo and ^{165}Ho [212]. The first bin corresponds to "minimal" annihilations, in which the antiproton annihilates with a proton or a neutron, but the remnant nucleus otherwise is unscathed. Right: Yield of residues after gold fragmentation by stopped antiprotons as a function of (a) atomic mass, (b) neutron number N and (c) atomic number Z.
Source: Reproduced from [206,208] with permission.

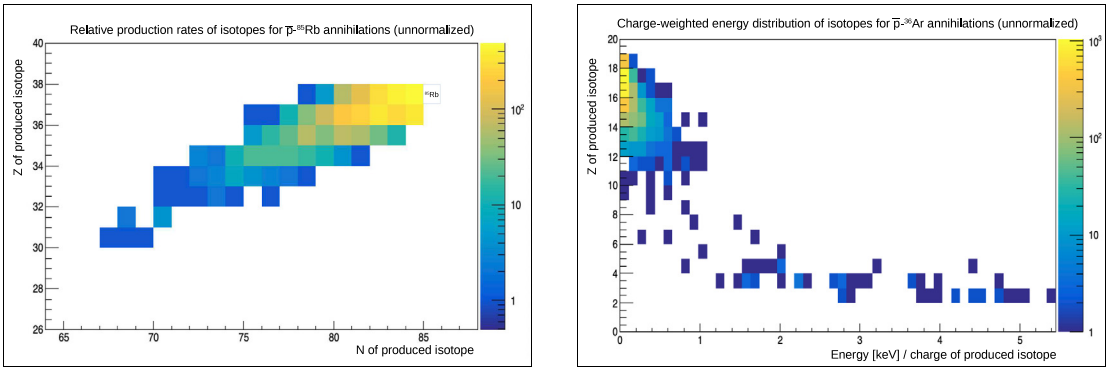

Fig. 13. Left: Relative production rates of radio-isotopes produced in Geant4 simulations of $\bar{p}-^{85}$Rb annihilations. Right: Relative rates of the charge-weighted energy (E [keV] / Q) of the produced Ar and lighter radio-isotopes [213] as a function of the nuclear charge Z of the remnant in $\bar{p}$-Ar annihilations. Peripheral annihilations, which lead to only small changes in Z or N, populate the low energy part of the energy distribution, particularly for heavy parent nuclei.

a wider nested trap, or by rapidly switching the polarity of the trap for negative particles concurrently with the pulsed photo-ionization and Rydberg excitation of the co-trapped anions.

It can thus be hoped that in at least some of these cases, the resulting ${}^{A-1}_{Z}A$ or ${}^{A-1}_{Z-1}A$ highly charged daughter nucleus will have a low enough recoil energy that may result in it remaining trapped. Indeed, the outcome of a simulation of range of antiprotonic atoms (see Fig. 13 for results for $\bar{p}$-Rb and $\bar{p}$-Ar) shows that the charge-weighted energy distribution of the produced radio-isotopes with $\Delta Z = 0$ or $\Delta Z = -1$ is low enough for moderate Penning trap electric fields of O(1 kV) to be sufficient to trap some of the (fully stripped) fragments if the precursor is not too light.

Any such highly charged trapped fragments can then form the basis for further studies, either of the fragments themselves, as detailed in the following, or as the starting point of hollow Rydberg atomic ions (see Section 6.1).

Formation (and peripheral annihilation) of antiprotonic atoms allows forming, with some degree of efficiency that remains to be determined but that simulations indicate can be quite sizable for heavy nuclei (up to 100% of the formation rate for kV trapping potentials), trappable highly charged radio-isotopes from trapped ions of stable or quasi-stable isotopes. In specific cases, this might then not only allow forming specific isotopes that are currently difficult to extract

Table 3
Selected annihilation reactions energetically compatible with $\bar{n}$ formation within or at the surface of the nucleus.

Reaction	Final state energy [u]	Lifetime of initial state isotope	Lifetime of final state isotope
^{7}Be + $\bar{p}$ → "^{8}Li"	0.0022u	53 d	839 ms
^{8}B + $\bar{p}$ → "^{9}Be"	0.0202u	730 ms	*stable*
^{11}C + $\bar{p}$ → "^{12}B"	0.0049u	20 m	20 ms
^{13}N + $\bar{p}$ → "^{14}C"	0.0103u	10 m	5730 y
^{24}Na + $\bar{p}$ → "^{25}Ne"	0.0004u	15h	0.6 s
^{33}P + $\bar{p}$ → "^{34}Si"	0.0004u	25 d	< 210 ns
^{40}Ca + $\bar{p}$ → "^{41}K"	0.008u	*stable*	*stable*
^{212}Rn + $\bar{p}$ → "^{213}At"	0.0051u	24 m	125 ns
^{216}Th + $\bar{p}$ → "^{217}Ac"	0.009u	27 ms	69 ns

Table 4
Selected annihilation reactions energetically compatible with free antineutron formation.

Reaction	Final state energy [u]	Lifetime of initial state isotope	Lifetime of final state isotope
^{8}B + $\bar{p}$ →^{8}Be + $\bar{n}$	0.0018u	770 ms	8 x 10^{-17}s
^{11}C + $\bar{p}$ →^{11}B + $\bar{n}$	0.0007u	20 m	*stable*
^{15}O + $\bar{p}$ →^{15}N + $\bar{n}$	0.0016u	122 s	*stable*
^{18}F + $\bar{p}$ →^{18}O + $\bar{n}$	0.0004u	109 m	*stable*
^{22}Na + $\bar{p}$ →^{22}Ne + $\bar{n}$	0.0015u	2.6 y	*stable*
^{211}Rn + $\bar{p}$ →^{211}At + $\bar{n}$	0.0013u	15 h	7 h
^{216}Th + $\bar{p}$ →^{216}Ac + $\bar{n}$	0.0009u	27 ms	0.4 ms

from production targets (e.g. F, Si, V, Zr, Nb, Mo, Tc, Ru, Rh, Ta, W, Re, Os, Ir, etc.) or that have very short lifetimes of the order of tens of ms (^{12}B, ^{13}B, ^{12}N) or even down to ns, but would furthermore ensure that they would be available inside a trap, thus potentially allowing subsequent manipulations or measurements. For heavier elements, this might also be a way to obtain very neutron rich isotopes of heavy elements. Under the assumption that only $\Delta(A) = -1$ transitions occur, then starting from trapped $^{196}Os^{+}$ (with a lifetime of 35 min), via this scheme, it should be possible to form trapped ^{195}Re, or from $^{190}W^{+}$ (with a lifetime of 30 m), to form trapped ^{189}Ta, or ^{225}At from $^{226}Rn^{+}$ (lifetime of 7.4 min), or ^{208}Au from $^{209}Hg^{+}$ (lifetime of 36 s). Whether reaching these states indeed requires starting from radioactive precursor states is currently being investigated via simulations; the outcome of these simulations in the case of Rb (Fig. 13) already indicates that a much broader set of precursor states, including stable or long-lived ones, can potentially result in a specific trapped neutron-rich radioisotope.

5.4.7. Antiprotonic atoms: antineutron production

While the process $\bar{p}p \rightarrow \bar{n}n$ is of course forbidden in isolation due to energy conservation, this is not necessarily the case for bound systems: the formation of an $\bar{n}n$ pair from a bound $\bar{p}p$ within a nucleus is energetically possible for a small number of nuclei, among them ^{7}Be:

$^{7}Be + \bar{p} \rightarrow$ "^{8}Li", with one of the neutrons of the "^{8}Li" being in fact an antineutron.

with m(^{7}Be) = 7.01692u, m(^{8}Li) = 8.02249u, this results in Δ(m[^{7}Be]+m[$\bar{p}$] - m[^{8}Li]) = 0.0022u. This process corresponding to $(5p + 3n) + \bar{p} \rightarrow (4p + 4n + n)$ is thus energetically allowed *if* the binding energy of the $\bar{n}$ is the same as that of the neutron; the observation of this process thus constitutes a test of CPT for the strong interaction. A clean tag for the presence of an antineutron (annihilation will most likely be immediate upon formation) is formed by measurement of the sum of charges of formed secondaries: $\Sigma_Q(\bar{n}p) = +1$, while all other annihilation processes result in a total charge of -1 ($\Sigma_Q(\bar{p}n) = -1$) or 0 ($\Sigma_Q(\bar{p}p) = 0$; $\Sigma_Q(\bar{n}n) = +0$). The process corresponds to:

${}^{A}_{Z}N + \bar{p} \rightarrow {}^{A+1}_{Z-1}N(\bar{n})$, where ${}^{A+1}_{Z-1}N(\bar{n})$ contains A neutrons and one antineutron.

Table 3 lists a number of such systems in which the reaction channel, available energy (in atomic units) and lifetimes of the mother and daughter isotopes are tabulated. Among these, the most sensitive probe is $^{24}Na + \bar{p} \rightarrow$ "^{25}Ne", with an energy difference of 0.0004u, e.g. 375 keV. Even more interestingly, a small number of radioisotope pairs have the characteristics required for a related process ${}^{A}_{Z}N + \bar{p} \rightarrow {}^{A}_{Z-1}N + \bar{n}$, i.e. for formation of a free antineutron. Here, the requirement is that $m(mother) > m(daughter) + 2m(n) - m(p)$).

Table 4 lists several reactions that should energetically be possible, and that would result in the release of a low energy antineutron (the lowest free energy occurring in the case of the reaction ^{18}F + $\bar{p}$ → ^{18}O + $\bar{n}$, with only 0.0004u being available above threshold; the resulting antineutron energy should thus be 375 keV). The potential availability of antineutrons with energies far below those of prior formation attempts through in-flight charge exchange ($E_{\bar{n}}$ > 100MeV [216]) opens up the intriguing possibility of measuring the antineutron annihilation cross section at very low $\bar{n}$ energies; such very low energy antineutron-nucleus data would be highly relevant for neutron–antineutron oscillation experiments [217].

Differentiating this process from the formation of an antineutron within the nucleus must rely, in addition to the total $\Sigma_Q(\bar{n}p) = +1$ of the produced mesons, on a timing difference between the last emitted atomic transition of the

antiprotonic atomic parent prior to annihilation and the detection of the antineutron annihilation. For an antineutron energy of 0.4 MeV, the velocity is 0.9 cm/ns, resulting in a temporal separation of $\sim$ 10 ns between the two signals for a 10 cm flight path. Additionally, the decay of the daughter nuclei can also be tagged if those are short-lived (^{8}Be, ^{216}Ac) or the daughter nucleus is identified via mass spectrometry in the case of longer-lived daughter nuclei. Admittedly, with the exception of ^{40}Ca and to some extent ^{22}Na, none of the precursor states can be considered stable. However, in all cases, only small numbers (O(10^6)) of radio-nuclei would be needed for pulsed production, resulting in very low amounts of released radiation.

5.4.8. Antiprotonic atoms of unstable isotopes

The formation scheme of hollow antiprotonic Rydberg ions $\bar{p}A^{(Z-1)+*}$, which relies on a finely tuned sequence of excitations and reactions, might also be a way to study nuclear relaxation processes that occur on the timescale of μs to ms after the annihilation process. Indeed, if they are formed immediately after production of the charged nuclear fragment, as is possible for pulsed formation, they could also allow investigating the trapped remnant's nuclear evolution from immediately after the annihilation event [218] via time-dependent precision spectroscopy. Similarly to the study of nuclear properties with muonic atoms [219–221], measurement of nuclear transitions that would occur on timescales comparable to slow atomic transitions in the hollow antiprotonic Rydberg ion would be a clean laboratory for nuclear relaxation processes that do not fragment the nucleus, and would furthermore also allow investigating the possible effect on the nuclear equation of state of the increasingly close antiproton in the course of its radiative cascade. Any such putative $\bar{p}$-induced tidal effects are perhaps best investigated with very narrow transitions, such as in the ^{229}Th system, as is being explored in muonic ^{229}Th [222]. Contrary to muonic atoms however, the interaction between the nucleus and a strongly interacting particle, in contrast to the only electromagnetically interacting muon, can be expected to play a rôle for the more deeply lying states, whose lifetimes are however very short. The benefit of antiprotonic atoms over muonic atoms thus resides on one hand in the feasibility of laser-controlled pulsed formation of cold systems, and on the other hand, in the significantly larger mass, and thus higher n state for comparable radial separation, for antiprotonic hollow ions. Together with time-resolved spectroscopy, pulsed formation in particular should be a powerful tool: it provides a well-defined starting point for observation of the atomic cascade of the initially molecule-like, and then increasingly nuclear-like system. Previous (time-integrating) observations of the transition X-rays would not have been sensitive to the temporal evolution of the system.

The cascade and spectroscopy of such antiprotonic atoms of unstable isotopes offers a further measurable similar to that of the antiprotonic atomic cascade (Section 5.4.3). Although it is difficult to extract absolute values for charge radii from the energies of the final states reached prior to annihilation, the obtained information on the nuclear charge radii of individual, even short-lived, radioisotopes, is perhaps most relevant for relative comparisons of different isotopes of the same element. Laser-spectroscopic investigations of their excited levels, similarly to (and complementary to) laser spectroscopy of e.g. muonic ^{9}Be [223], but extendable to ^{7}Be, ^{10}Be, etc. can also be contemplated. These must however address challenges concerning not only the question of the impact of nuclear form factors on these large-radius states, but also propose a methodology for inducing narrowband and identifiable transitions between two Rydberg states, for which some proposals were outlined in Section 5.4.3.

Simulations of the annihilation process leading to the final (trapped) nuclear fragments are insufficiently precise to be able to predict the relative formation rates for ground and isomeric states, which will need to remain an experimental question. It can be hoped that the ratios of produced isomers to ground state radioisotopes will differ from those of the alternative production channels of radioactive decay and spallation, as the nuclear processes involved are different. In any case, any isomeric states will, in case they are formed, be trapped together with the ground states and be amenable to mass spectrometry, as has been carried out for a wide range of known isomers in Penning traps [224], including relatively short-lived (down to 17.9 ms) isomers [225]. Given the pulsed nature of the formation process, a similar scheme (also without formation of an antiprotonic Rydberg atom after the initial annihilation) is feasible, thereby in principle allowing access to even shorter lifetimes.

6. Antiprotonic ions

Given the difficulty in trapping (neutral) antihydrogen atoms, it is natural that alternative, easier to trap, charged bound antimatter systems have been considered. The most prominent of these is the antimatter analog to the H^- ion: $\bar{H}^+$. An early molecular dynamics simulation of the formation of $\bar{H}$ in combined plasmas of $\bar{p}$ and e^+ in strong magnetic fields [226] also identified formation of a small fraction (a few % relative to the formed $\bar{H}$) of $\bar{H}^+$ ions. A recent detailed calculation of the same process [227] provides a quantitative value of 5×10^{-7} s^{-1} $\bar{H}^+$ per antihydrogen atom interacting with cold positrons, which would lead a handful such ions per day in the ALPHA experiment. This process can however be improved upon: in particular laser-induced radiative attachment [228] of positrons to (trapped) $\bar{H}$ can significantly enhance the formation rate of $\bar{H}^+$.

A different formation mechanism for this ion which constitutes the heart of the GBAR experiment [229] proceeds via a double charge exchange process between a $\bar{p}$ and two positronium atoms [76]:

$$\bar{p} + Ps \rightarrow \bar{H} + e^-;$$
$$\bar{H} + Ps \rightarrow \bar{H}^+ + e^-$$

While in this scheme, Ps is in the ground state, the formation cross section can be improved by exciting Ps from the ground state into Ps(n=2). While a first investigation also indicated an even greater formation cross section for Ps(n=3) [230], a more recent *ab initio* calculation [231] finds that close to the threshold energy, the cross section for the formation of $\bar{H}^+$ in the collision of Ps(nl) + $\bar{H}(1s)$ is actually largest for n=2, followed by n=1 and n=3.

While the $\bar{H}^+$ ion is stable and is thus amenable to investigation, a number of further systems are likely not accessible to experimentation, in spite of their interest, due to their very short lifetimes (if they even exist), or the possible absence of a bound state. Ignoring for a moment the former question, the stability of few-charge systems, several of which are of interest here, has been investigated in [232]. An analogous system to the $\bar{H}^+$ ion is obtained when replacing the antihydrogen atom with a protonium atom: the protonic or antiprotonic analog to Ps^-, ($pp\bar{p}$) or ($\bar{p}p\bar{p}$), should follow the same stability arguments as Ps^-, and thus form a (most likely very short lived) bound state. Indeed, Mitroy [233] showed that the ionic combination (m_1^+, m_2^+, m_2^-) of two species is stable if

$$0.698 \leq \frac{m_1}{m_2} \leq 1.63 \tag{12}$$

a condition satisfied by ($\bar{p}p\bar{p}$), but not, on the other hand, by the combination d$\bar{p}$p (which requires the presence of a fourth particle, a $\bar{d}$, to be stabilized into a molecular state). The study of the ($\bar{p}p\bar{p}$) system, which is stable with Coulomb forces only, would allow investigating the long-range part of the strong interaction between a proton and an antiproton.

The binding energy of a hypothetical ($\bar{p}pe^-$) ion, a bound state of a protonium atom (1S) and an electron (or a positron), has been evaluated [234], and found to be −0.08793 eV in the ground state, in disagreement with a calculation based on the hyperspherical coordinate method [235], which finds that the protonium negative (or positive) ion does not exist and that there are no excited resonant states of such an ion for principal quantum numbers below n=30. While the possible existence of an ion of ground state protonium is somewhat academic, given the very high likelihood of proton–antiproton annihilation from the 2P level, the existence (or not) of an ion of a Rydberg state of protonium requires somewhat more discussion. As shown in [232], the dipole polarizability of the "central" (p, $\bar{p}$) atom plays a key role. While for ground state protonium, the dipole is extremely small (and in the extreme case of a point-like protonium atom would not have a charge with which to bind an electron), this is different for protonium in Rydberg states. In the case of H^-, the configuration of the first electron is very similar to protonium in n $\sim$ 40 and thus comparable polarizability as ground state Hydrogen; this hints at the possibility of stable configurations with the antiproton in n $\sim$ 40, with lifetimes of μs, and an electron (corresponding to the second (outer) electron of H^-) at a greater radial separation. Such a state, however, will not be stable against Auger emission, since the normalized radial orbitals of H^-, in spite of having different fall-offs towards large radial distances from the proton [236], also have a substantial overlap at low radial distances.

As indicated in Section 5.2, heavier $\bar{p}A^{+++*}$ ionic atoms can be formed by injecting antiprotons into a plasma of (possibly laser-cooled) positive ions (Eq. (7)), which will remain trapped within the positively charged ionic environment in which they are formed. If needed, the sample could be purified by removing the non-antiprotonic atomic ions from the trap by appropriate application of RF, which however requires a sufficient lifetime of the antiprotonic atomic ion. This will only be the case if the ions are in Rydberg states prior to their interaction with antiprotons, which however is difficult to achieve in the case of 3-body interactions: in this process, the moment of formation is defined by the time the injected antiprotons require to thermalize with the trapped ions, which can be quite lengthy.

It might thus be more interesting, albeit quite daunting, to begin with co-trapped anions and antiprotons:

$$A^- + \gamma_1 \rightarrow A_g + e^- \qquad \text{(photo-neutralization)} \tag{13}$$

$$A_g + \gamma_2 \rightarrow A_e \qquad \text{(excitation of the neutral atom)} \tag{14}$$

$$A_e + \gamma_3 \rightarrow A^+ + e^- \qquad \text{(photo-ionization)} \tag{15}$$

$$A^+ + \gamma_4 \rightarrow A_e^+ \qquad \text{(excitation of the cationic atom)} \tag{16}$$

$$A_e^+ + \gamma_5 \rightarrow A_n^{*+} \qquad \text{(Rydberg excitation of the cationic atom)} \tag{17}$$

$$A_n^{*+} + \bar{p} \rightarrow \bar{p}A_{n'}^{*++} + e^- \qquad \text{(formation of the Rydberg antiprotonic ion)} \tag{18}$$

The resulting singly charged Rydberg antiprotonic ions will require a nested well to remain trapped. Furthermore, their temperature will be higher than those formed in 3-body interactions, but their long lifetimes should provide ample time for subsequent manipulations.

6.1. Formation of highly charged, hollow antiprotonic rydberg atomic ions

Although well beyond current possibilities, since neither pulsed formation of antiprotonic atoms nor trapping of the resulting nuclear remnant ions has been established, it is possible to build on the proposed production and trapping of nuclear remnants detailed in Section 5.4.6 by – in a second step – "dressing" these highly charged fragments or nuclear remnants with a second antiproton. Since the moment of production of any trappable daughter nuclei or nuclear fragments is known to a few ns, one can reiterate the initial formation process. However, contrary to the first step, in which one of the electrons of the trapped charged ion could be excited into a Rydberg state (after photo-neutralization of the ion), the trapped charged fragments A^{Z+} have no (or only very deeply) bound electrons. Instead, a charge exchange process can

be implemented with Rydberg atoms produced in the vicinity of the trapped fragments. As indicated in Section 5.2, such charge exchange processes between ions and Rydberg atoms result in new Rydberg systems in states similar to those of the original Rydberg atom [147]. Three possible processes are easily imaginable:

$$A^{Z+} + B^* \rightarrow A^{(Z-1)+*} + B^{+*} \tag{19}$$

$$A^{Z+} + Ps^* \rightarrow A^{(Z-1)+*} + e^+ \tag{20}$$

$$A^{Z+} + \bar{p}p^* \rightarrow \bar{p}A^{(Z-1)+*} + e^- + p \tag{21}$$

The first would start from B^- ions trapped in the vicinity, which are first photo-ionized, and subsequently excited into a Rydberg state; the second would mimic the pulsed production process of antihydrogen [36] to form the same hollow Rydberg ion $A^{(Z-1)+*}$. The third process builds on a charge exchange process with protonium atoms formed shortly after production of the A^{Z+*} fragment from nearby co-trapped H^- and $\bar{p}$ [94]. Those Rydberg protonium atoms[1] can then lead, via a second charge exchange process, to (hollow) Rydberg antiprotonic atoms consisting of the daughter or nuclear fragment and the antiproton. This process is similar to the interaction between antiprotons and highly charged ions in an electron beam ion trap [237], which has been found to have a very high cross section. Alternatively, injecting $\bar{p}$'s into trapped positive ions would equally lead to formation of antiprotonic Rydberg cations, mainly via three-body interactions involving an electron of the positive ion, and very occasionally involving a second positive ion (see Eq. (1)), albeit continuously and with no control over the resulting Rydberg state.

These (highly charged, trapped) hollow Rydberg ions are essentially heavy charged ions with a single negative particle, an electron or an antiproton, in a long-lived Rydberg state (for antiprotonic atoms heavier than Kr, the K-shell electrons could still be present, while for lighter atoms, they will have been completely removed in the preceding cascade). They are thus perfect systems for high resolution spectroscopic investigations of QED in the strong field regime [238], in analogy to studies of hollow atoms [239], such as those that can be produced with highly charged heavy ions [238]. Such hollow antiprotonic Rydberg ions $\bar{p}A^{(Z-1)+*}$ however also offer a route towards alternative and improved measurements of the antiprotonic Rydberg constant via the spectroscopy of circular, high-n Rydberg states, similar to the approach being taken in one-electron medium-Z ions [240], which are insensitive to both QED and finite nuclear size corrections.

7. Antiprotonic molecules

A small number of neutral antiprotonic molecules are of particular interest: the antihydrogen molecule $\bar{H}_2$, the positronium antihydride molecule Ps$\bar{H}$, and the protonium molecule Pn_2, all of which are stable if the interactions are purely Coulombic. Similarly, also Ps_2 forms stable molecular states. As shown by [232], while a PsH (and thus a Ps$\bar{H}$) state is stable, the H-$\bar{H}$ state is not, although this has not yet been rigorously proven. The result of a more general investigation [241] of pairs of (M^+, M^-) and (m^+,m^-) particles via a variational Monte Carlo method [242] is that for $M/m \gtrsim 2$, no bound state of the system exists, a condition clearly satisfied in the case of $\bar{H} - H$ with $M/m = 1836$.

Given the respective short lifetimes of the ground states of the constituents of Pn_2 and of Ps$\bar{H}$, of more interest is the question whether they might also be stable as a molecule of Rydberg states: in order for any of these systems to be used in high-precision experiments to test CPT or measure the antiproton–proton interaction at distances well in excess of the nm scale, protonium atoms and molecules containing them must rely on long-lived Rydberg states. For these systems, although no experimental investigations have taken place yet, the existence of similar long-lived molecules of Rydberg atoms, or of Rydberg molecules, is encouraging. Specifically, molecular analogs to a putative Rydberg–Rydberg molecule $(\bar{p}p)^*(\bar{p}p)^*$ exist and exhibit a rich spectrum [243]; this has also been predicted for the positronium molecule Ps_2 [244]. Formation of these would require starting with a relatively cold and dense ensemble of $(\bar{p}p)^*$, such as is the case for pulsed production of Pn; even under those conditions however, the formation cross section, in spite of the long-distance dipole–dipole interactions between the Rydberg atoms, is low.

As such, the only ground state, stable antiprotonic molecule that it is currently envisageable to study is $\bar{H}_2$. Formation of such a molecule is most likely to proceed via the association of two ground state $\bar{H}$ atoms, although as for the formation of the antihydrogen atoms themselves, carrying off the molecular binding energy will require either a three-body interaction or the absorption of a photon from an applied laser field during the collision. Formation of molecules via the intermediate formation of Feshbach molecules has been achieved for bi-alkali systems [245,246]; implementing this approach to the formation of $\bar{H}_2$ will require large numbers of cold, trapped antihydrogen atoms. Alternatively, assuming that production of the $(\bar{H})^+$ ion is successfully implemented, interacting these within a nested Penning trap with antiprotons should lead – via three body interactions – to the formation of $\bar{H}_2$ in excited states.

A completely different type of molecule is formed when the antiproton replaces an electron in an existing molecular system. Unless this system is formed from a Rydberg molecule, cascade processes involving Auger emission, analogous to those in atoms, will take place, with the antiproton ending up forming an antiprotonic atom with which it subsequently annihilates. Lifetime arguments from antiprotonic atoms ($\tau \sim$ ns) carry over to antiprotonic molecules; only Rydberg antiprotonic molecules would be expected to have similarly extended lifetimes as Rydberg antiprotonic atoms.

[1] Naturally, the same production mechanism would also be feasible with $\bar{H}^*$, but production rates of protonium from co-trapped H^- and $\bar{p}$ should be significantly larger.

The study of muonic molecules provides some unexpected insights which point towards intriguing, if remote, possibilities in the case of antiprotons. Particularly the observation of differences between the behavior of muonic systems building on graphite or diamond on one hand, and those on the fullerene C_{60} on the other hint at the existence of the formation of a bound state between a carbon atom and a muon at the center of a rearranged C_{58} cage [247]. Although in the case of antiprotons, the lifetime such an encapsulated antiprotonic would be no different from that of a free antiprotonic carbon atom, formation of such a system could allow shedding light on the encapsulation and electron-sharing processes that have been observed for endohedral atoms [248], cations [249] and even anions [250] in fullerenes.

7.1. Antiprotonic ionic molecules

The differentiation between atomic ion and ionic molecule becomes blurred when considering attaching antiprotons to atoms. This is the case when antiprotons are attached to e.g. hydrogen, antihydrogen or protonium, resulting in (p, $\bar{p}$, e^-), ($\bar{p}$, $\bar{p}$, e^+) and (p, $\bar{p}$, $\bar{p}$) systems, as discussed above. Among more complex molecular systems, particularly the $\bar{H}_2^-$ ionic molecule holds great interest for precision measurements: such ionic antihydrogen molecules are the antimatter analog to the highly interesting H_2^+ (and HD^+) molecules that are candidates for highly accurate (systematic uncertainty at the level of 10^{-16}) molecular clocks [251] and that would allow tests of CPT [252,253] that are very competitive with 1s-2s and hyperfine spectroscopy of antihydrogen atoms.

The production of such complex systems is significantly more challenging than formation of antiprotonic atoms or of antihydrogen, and to date, no formation mechanism has been established for them, although a number of routes (detailed below) have been proposed. The first such approach based on associative detachment:

$$\bar{H}^+(nLS) + \bar{p} \rightarrow \bar{H}_2^- + e^+. \tag{22}$$

is discussed by Myers for both matter and antimatter systems [253]; the resulting cross section is however low, and furthermore, obtention of the requisite $\bar{H}^+$ technologically highly demanding: only very low production rates for this ion are expected by the only experiment (GBAR [74]) currently focusing on its production. Two other processes relying only on more readily available antihydrogen atoms and antiprotons (radiative association and associative ionization) will be discussed below.

In the previous sections, pulsed formation of antiprotonic Rydberg atoms was discussed, starting from a mixed system consisting of an atomic anion and antiprotons trapped within the same Penning trap. This scheme can be expanded to multiple co-trapped anionic species, thus opening further intriguing possibilities. Consider an ensemble of three co-trapped anionic species: antiprotons, Cs^- and H^-. Simultaneous pulsed formation of Rydberg antihydrogen, antiprotonic cesium Rydberg atoms and Rydberg protonium leads to the possibility of interactions between two species of Rydberg atoms via associative ionization:

$$\bar{p}Cs^* + \bar{p}p^* \rightarrow \bar{p}\bar{p}p^* + Cs^+ \tag{23}$$

which would result in a system analogous to (excited states of) Ps^-, resp. Ps^+ (the question of the existence of such states is discussed in [254]). Similarly, simultaneous formation of Rydberg antihydrogen and of Rydberg protonium,

$$\bar{H}^* + \bar{p}p^* \rightarrow \bar{H}_2^{-*} + p \tag{24}$$

or of two simultaneously formed Rydberg antihydrogen atoms

$$\bar{H}(nl) + \bar{H}(n'l') \rightarrow \bar{H}_2^{-*} + e^+ \tag{25}$$

would result in the formation of an excited state of the antihydrogen molecular ion $\bar{H}_2^{-*}$. While formation rates of that ion via these processes may well be low, a number of techniques stemming from ultra-cold molecule formation, such as careful tuning of the parameters of associative ionization (among them the internal states of the formed Rydberg atoms or their relative momenta), might help increase the yields. It should however be noted that associative ionization between two excited states is less than one tenth of the Penning ionization [255] in which two Rydberg antihydrogen atoms would dissociate into an antiproton, a positron and an antihydrogen atom in a changed (n,l) configuration.

Any such antihydrogen molecular ions would, in the formation scheme that requires co-trapped negatively charged "ingredients", remain trapped, thus allowing accumulation even in the case of very low formation rates per attempt; similarly, any antiprotons resulting from Penning ionization would remain trapped, and could consequently be reused for subsequent formation attempts.

An alternative path to form this molecular ion could be, in the same negatively charged particle trap, to attempt a photo-associative Raman process (STIRAP) to combine a Rydberg atom and an ion (in this case, an antiproton) into a molecular ion, analogously to the formation of $(LiCs)^+$ from Li and Cs^+ [256]:

$$\bar{H}^* + \bar{p} + \gamma + \gamma \rightarrow \bar{H}_2^{-*} \tag{26}$$

The same associative detachment scheme might allow forming even more complex systems *ab initio*, with the potential of then using those to probe heretofore unmeasured properties of antiprotons, such as the antiproton's electric dipole

moment $\bar{p}$EDM (which should of course be almost zero in the Standard Model), via spectroscopy of specific antiprotonic Rydberg molecules $\bar{p}AB^*$, starting from two anionic species A^- and B^- co-trapped with antiprotons:

$$A^- + \gamma_1 \rightarrow A_g + e^-; A_g + \gamma_2 \rightarrow A_e; A_e + \gamma_3 \rightarrow A_n \tag{27}$$

$$A_n + \bar{p} \rightarrow \bar{p}A^*_{n1} + e^- \tag{28}$$

$$B^- + \gamma'_1 \rightarrow B_g + e^-; B_g + \gamma'_2 \rightarrow B_e; B_e + \gamma'_3 \rightarrow B_{n2} \tag{29}$$

$$B_{n2} + \bar{p}A^*_{n1} \rightarrow \bar{p}AB^* \tag{30}$$

Naturally, a scheme starting from trapped ground state antihydrogen atoms can also be envisaged; formation of molecular $\bar{H}_2^-$ both via radiative association of cold trapped antihydrogen atoms with antiprotons (analogously to the radiative association of p and H [257]) or via associative ionization among trapped antihydrogen atoms, with possibly prior excitation into states with $n \geq 2$ to increase the formation cross section, has been investigated by Zammit [258]. While pulse-formed antihydrogen atoms are already in Rydberg states, photo-excitation of trapped ground state antihydrogen atoms must also evaluate the possibility of spin-flip induced losses of trapped $\bar{H}$, thus setting a limit to the number of possible interactions a given trapped $\bar{H}$ can potentially undergo before being lost from the trap. In spite of this limitation, production rates for the molecular ion $\bar{H}_2^-$ under reasonable extensions of existing technologies of 10's of trapped $\bar{H}_2^-$ per hour appear possible. Such numbers should already be sufficient in order to carry out precision spectroscopy of these trapped molecular ions, and first experiments on them have been proposed [259].

Finally, even more complex, but also stable [232] systems can be envisaged, such as $(e^+e^-e^+e^-\bar{p})$, a system made of a Ps_2 molecule and an antiproton, or the trihydrogen H_3^- molecular ion consisting of three $\bar{p}$ and two electrons, which would represent the antimatter analog for the simplest and most fundamental polyatomic system H_3^+, and a unique antimatter system whose energy levels allow probing the onset of chaos in a molecular system [260] or testing [261] the validity of selection rules for a quantum number G (introduced in the context of symmetric-top molecules'[262] and built from the angular momentum around the top axis (quantum number k) and l (vibrational angular momentum)) that is tied to the molecule's Pauli-principle defined symmetry. Forming $\bar{H}_3^-$ would be even more challenging than forming $\bar{H}_2^-$, and would presumably require having formed the later before associating an antihydrogen atom to it.

A further, but related, intriguing mixed-matter system is the antiproton–deuteron–triton ion, studied by Armour [263] as part of an investigation of the stability of 3-body atomic and molecular ions containing electrons (positrons), (anti)muons or (anti)protons (which showed inter alia that e^+Pn or $e\bar{p}\mu$ are not bound, but μPn is), and more specifically by Frolov [264]. This system, since it contains three heavy particles, is unique among all Coulomb three-body systems with unit charges, but only has a very small binding energy and thus only a single stable (ground) state (with 12 levels of hyperfine structure). Given its very small spatial extent of only about 50 times the effective nucleon–nucleon interaction distance, it is a very sensitive probe of the inter-particle potentials. Furthermore, two annihilation channels are open to this molecular ion: antiproton–nucleon annihilation; and (antiproton-catalyzed) (d, t) fusion. In spite of its expected lifetime of less than 10^{-14} s, this system can be very interesting in studying long-range asymptotics of the strong interaction, as the specifics of the molecular ion's properties are highly sensitive to the detailed interaction potentials. Forming such a (short-lived) ion might start from the molecular hydrogen isotope DT, and then proceeding as with H_2: ionization to form H_2^+, resp. DT^+, which are trapped and then mixed with antiprotons, to form $(pp\bar{p})$, resp. $(\bar{p}dt)$. Given the very small overlap between the wave functions of the $\bar{p} - d - t$ system and that of the $\bar{p}$-DT^+ molecular system, the formation rate can however be expected to be extremely low, and this approach to mainly lead to $\bar{p}d$ or $\bar{p}t$, with the other nucleus being ejected in the course of the cascade.

Further antiprotonic molecular systems have not yet been discussed in the literature to any significant extent, although a number of intriguing and novel, both cationic and anionic, systems are worthy of consideration. In both cases, only potentially long-lived states will be discussed in the following.

7.1.1. Cationic antiprotonic systems

Formation of antiprotonic Rydberg ions patterned on the three-body production of Rydberg antiprotonic atoms, building on antiprotons injected into trapped Rydberg ions, should be feasible as long as such trapped Rydberg ions are available. In a detailed theoretical and conceptual feasibility study [265], followed by the experimental demonstration of excitation of a single trapped cold $^{40}Ca^+$ ion to Rydberg levels [266], Schmid-Kahler and co-workers could establish the feasibility of the production of trapped Rydberg (atomic) ions, albeit in Paul traps, which should be extendable to other (atomic or molecular) ionic systems. Such trapped Rydberg ions are of interest for the study of their interactions in Coulomb crystals, and particularly relevant for quantum simulations and the implementation of quantum gates'[267,268]. With their expected long lifetimes, antiprotonic Rydberg cations should similarly be produceable and trappable (in double-well Penning traps) and even sympathetically coolable with, e.g. laser-cooled Be^+. Obtaining cold antiprotons from this approach is nonetheless challenging, since any photo-detached antiprotons would still be located within the same double-well Penning trap, however with high energy with respect to the minimum of the potential for negative species unless the double-well Penning trap were to be transformed, after formation of the cation, into a single well Penning trap and the released low energy antiprotons reused immediately after photo-detachment.

An even more ambitious system consisting of a Rydberg antiprotonic atom interacting with a positive atomic ion to form a long-range atom–ion Rydberg molecule [269], exemplified by the long-range Rydberg atom–ion molecule

consisting of Rb* or Cs* and e.g. Hg^+, Sr^+ or Yb^+ [270], of Rb atoms and alkaline-earth ions (Ca^+, Sr^+, Ba^+) or of Li and Yb^+ [271] and formed via resonant photo-association, is also imaginable, although the many steps to ensure the simultaneous formation of the antiprotonic Rydberg atom and of the atomic ion, all starting from co-trapped anionic species, and then forming the ionic antiprotonic Rydberg molecule are quite daunting.

7.1.2. Anionic antiprotonic molecules

Polar molecules (and their clusters) may bind an excess electron, which has little spatial overlap with the neutral molecules' valence electrons. Obtaining a complete description of the electron binding of such anionic molecules requires inclusion of electron correlations between the excess electron and the full set of electrons of the neutral molecule [272] and it is thus of interest to investigate the effect of replacing the excess electron with an antiproton. Although long-lived anionic molecules are abundant in space (e.g. C_6H^- [273,274]), the replacement of the supernumerary electron by an antiproton is unlikely to form a molecular anion that is stable on timescales that are long with respect to Auger emission by the antiproton of one of the valence electrons. Alternatively, formation of a long-range atom–ion Rydberg molecule with a negative ion, in this case the antiproton, may be possible [270], but will require ultra-cold antiprotons. The situation might however be different in magnetic fields, as magnetically induced anions [275] - with a rich spectrum of bound states — are known to exist.

Alternatively, and although *stricto sensu* not an anionic molecule, attempting to replicate the investigations of negative ion resonances obtained by interacting a neutral ground-state atom with the Rydberg electron of a Rydberg atom in ultra-long range Rydberg molecules (ULRM) [276] can be envisaged also with the antiproton playing the role of the Rydberg electron: the analogous system would then be that of a neutral atom embedded in, or interacting with, an antiprotonic Rydberg atom. Should it be possible to form such a system, e.g. via a charge-exchange process involving a normal atom and a Rydberg antiprotonic atom, this would then allow investigating the resonances of an antiprotonic anion or sub-threshold antiproton-neutral atom scattering at collision energies in the meV range [277]. In particular, details of the spin–orbit coupling of the Rydberg antiproton and the ground state atom can be revealed in such a system. Furthermore, a rich spectrum of trilobite, of butterfly or of ultra long-range giant dipole ULRM's in polyatomic ULRM's provide on one hand tuneability, and on the other hand, the potential of observing dynamical processes and makes these systems particularly interesting. Sufficiently long lifetimes of tens of μs, and up to the lifetimes of the Rydberg atoms themselves, have been achieved in specific ULRM's which thus allow such investigations, but their formation has required starting from ultra-cold relatively dense atomic ensembles; determining the feasibility of forming even minute numbers of antiprotonic ULRM's will remain a challenge for many years.

8. Outlook

Rapid advances in the last decade in formation, trapping and manipulation of antihydrogen, as well as longer term developments of high resolution spectroscopic investigations of $\bar{p}$-He atoms, together with recently initiated attempts to form antiprotonic atoms of radio-isotopes or antiprotonic ions are coming together to allow a significant growth in the number and configurations of increasingly complex antiprotonic systems that are amenable to study. Investigations of these systems that allow addressing a wide range of physics topics, from tests of fundamental symmetries to searches for beyond-the -standard-model physics to novel approaches to open questions in nuclear physics, are becoming feasible, and the coming decade should see a significant growth in activity, both in breadth in the number of systems that become available as well as in sensitivity, as techniques from atomic, molecular and nuclear physics are combined with those of trapping, cooling and manipulating positrons and antiprotons.

Declaration of competing interest

The authors declare that they have no known competing financial interests or personal relationships that could have appeared to influence the work reported in this paper.

References

[1] N. Paul, et al., Phys. Rev. Lett. 126 (2021) 173001.
[2] W. Krolokowski, R. Sosnowski, S. Wycech, Acta Phys. Polon. B 21 (1990) 717–722;
M.S. Safronova, D. Budker, D. DeMille, Derek F. Jackson Kimball, A. Derevianko, Charles W. Clark, Rev. Mod. Phys. 90 (2018).
[3] A. Obertelli, et al., Probing the Density Tail of Radioactive Nuclei with Antiprotons, Letter of Intent CERN-INTC-2017-097 ; INTC-I-206, 2017.
[4] D. Colladay, V.A. Kostelecký, Phys. Rev. D 55 (1997) 6760–6774.
[5] D. Colladay, V.A. Kostelecký, Phys. Rev. D 58 (1988) 116002.
[6] G. von Dardel, et al., PRL 5 (1960) 333.
[7] W. Bartmann, et al., Trans. R. Soc. 376 (2018) 20170266.
[8] H. Poth, Nuclear Phys. A 478 (1988) 655c–664c.
[9] G. Backenstoss, Contemp. Phys. 30 (1989) 433–448.
[10] C.J. Batty, Rep. Progr. Phys. 52 (1989) 1165.
[11] D. Gotta, Prog. Part. Nucl. Phys. 52 (2004) 133–195.
[12] M. Hori, J. Walz, Prog. Part. Nucl. Phys. 72 (2013) 206–253.
[13] J.-M. Richard, Front. Phys. (2020) http://dx.doi.org/10.3389/fphy.2020.00006.

[14] Y. Yamazaki, Proc. Jap. Academy, Ser. B 96 (10) (2020) 471–501, http://dx.doi.org/10.2183/pjab.96.034.
[15] J.S. Cohen, N.T. Padial, Phys. Rev. A 41 (1990) 3460.
[16] B. Desai, Phys. Rev. 119 (1960) 1385.
[17] G. Gabrielse, et al., Phys. Rev. Lett. 57 (1986) 2504.
[18] L. Venturelli, et al., ATHENA collaboration, NIM B 261 (2007) 40–43.
[19] J.S. Cohen, Phys. Rev. A 56 (1997) 3583–3596.
[20] K. Sakimoto, J. Phys. B: At. Mol. Opt. Phys. 34 (2001) 1769–1782.
[21] S. Jonsell, Phil. Trans. R. Soc. A 376 (2018) 20170271.
[22] D. Krasnický, R. Caravita, C. Canali, G. Testera, Phys. Rev. A 94 (2016) 022714;
D. Krasnický, et al., J. Phys. B: At. Mol. Opt. Phys. 52 (2019) 115202.
[23] G. Gabrielse, S.L. Rolston, L. Haarsma, W. Kells, Phys. Lett. A 129 (1988) 38.
[24] J. Cohen, Phys. Rev. A 69 (2004) 022501.
[25] J.S. Cohen, Phys. Rev. A 62 (2000) 022512.
[26] C. Surko, et al., Phys. Rev. Lett. 62 (1989) 901.
[27] G. Baur, et al., Cern/SPSLC 94-29 1994, p. P283.
[28] G. Baur, et al., Phys. Lett. B 368 (1996) 251.
[29] G. Blanford, et al., Phys. Rev. Lett. 80 (1998) 3037.
[30] M. Amoretti, et al., Nature 419 (2002) 456–459.
[31] G. Gabrielse, et al., Phys. Rev. Lett. 89 (2002) 213401.
[32] G. Gabrielse, et al., Phys. Rev. Lett. 89 (2002) 233401.
[33] S. Jonsell, et al., J. Phys. B: At. Mol. Opt. Phys. 42 (2009) 215002.
[34] N. Kuroda, S. Ulmer, D.J. Murtagh, et al., Hyp. Int. 235 (2015) 13–20.
[35] N. Kuroda, S. Ulmer, D. Murtagh, et al., Nature Commun. 5 (2014) 3089.
[36] C. Amsler, et al., AEgIS coll., Comm. Phys. 4 (19) (2021).
[37] M. Antonello, A. Belov, G. Bonomi, R.S. Brusa, M. Caccia, et al., Phys. Rev. A 102 (2020) 013101;
K. Shu, A. Ishida, T. Namba, S. Asai, N. Oshima, B. O'Rourke, K. Ito, Phys. Rev. A 104 (2021) L050801.
[38] C.H. Storry, et al., ATRAP collaboration, Phys. Rev. Lett. 93 (2004) 263401.
[39] G. Gabrielse, et al., Phys. Rev. Lett. 93 (2004) 073401.
[40] G.B. Andresen, et al., ALPHA coll., Nature 468 (2010) 673–676.
[41] G. Gabrielse, et al., Phys. Rev. Lett. 108 (2012) 113002.
[42] G. Gabrielse, et al., ATRAP coll., Phys. Rev. Lett. 100 (2008) 113001.
[43] G.B. Andresen, et al., ALPHA coll., Nat. Phys. 7 (2011) 558–564.
[44] B.M. Jelenkovics, A.S. Newbury, J/J. Bollinger, W.M. Itano, T.B. Mitchell, Phys. Rev. A 67 (2003) 063406.
[45] C.J. Baker, et al., ALPHA coll., Nat. Commun. 12 (2021) 6139.
[46] M. Ahmadi, et al., ALPHA coll., Nat. Commun. 8 (2017) 681.
[47] Y. Yamazaki, M. Doser, P. Perez, Antihydrogen Beams, ISBN: 978-0-7503-2021-4, 2018, http://dx.doi.org/10.1088/978-0-7503-2021-4.
[48] AEgIS proposal: http://cds.cern.ch/record/1037532/files/spsc-2007-017.pdf.
[49] N. Madsen, M. Charlton, New J. Phys. 23 (2021) 073003.
[50] B. Kolbinger, et al., Eur. Phys. J. D 75 (2021) 91.
[51] B. Radics, D.J. Murtagh, Y. Yamazaki, F. Robicheaux, Phys. Rev. A 90 (2014) 032704.
[52] B. Radics, Y. Yamazaki, J. Phys. B 49 (2016) 064007.
[53] T. Wolz, C. Malbrunot, M. Vieille-Grosjean, D. Comparat, Phys. Rev. A 101 (2020) 043412.
[54] E. Vliegen, S.D. Hogan, H. Schmutz, F. Merkt, Phys. Rev. A 76 (2007) 023405.
[55] U. Eichmann, T. Nubbemeyer, H. Rottke, et al., Nature 461 (2009) 1261–1264.
[56] C.J. Baker, et al., ALPHA coll., Nature 592 (2021) 35–42.
[57] C.G. Parthey, et al., Phys. Rev. Lett. 107 (2011) 203001.
[58] C. Amole, et al., ALPHA coll., Nature 483 (2012) 439.
[59] M. Ahmadi, et al., ALPHA coll., Nature 548 (2017) 66–69.
[60] M. Ahmadi, et al., ALPHA coll., Nature 557 (2018) 71–75.
[61] P. Crivelli, D. Cooke, M.W. Heiss, Phys. Rev. D 94 (2016) 052008.
[62] V.A. Kostelecký, A.J. Vargas, Phys. Rev. D 92 (2015) 056002.
[63] A. Grinin, A. Matveev, D.C. Yost, L. Maisenbacher, V. Wirthl, R. Pohl, T.W. Hänsch, T. Udem, Science 370 (6520) (2020) 1061–1066.
[64] O. Arnoult, F. Nez, L. Julien, F. Biraben, Eur. Phys. J. D 60 (2010) 243–256.
[65] M. Ahmadi, B.X.R. Alves, et al., ALPHA coll., Nature 578 (2020) 375–380.
[66] N. Kuroda, et al., J. Phys.: Conf. Ser. 875 (2017) 022054.
[67] G. Newton, D.A. Andrews, P.J. Unsworth, Phil. Trans. R. Soc. A 290 (1979) 373.
[68] V.A. Kostelecký, J.D. Tasson, Phys. Rev. D 83 (2011) 016013.
[69] G. Gabrielse, A. Khabbaz, D. Hall, C. Heimann, H. Kalinowsky, W. Jhe, Phys. Rev. Lett. 82 (1999) 3198–3201.
[70] S. Ulmer, et al., Nature 524 (2015) 196–199.
[71] M.A. Hohensee, H. Müller, R.B. Wiringa, Phys. Rev. Lett. 111 (2013) 151102;
M.A. Hohensee, S. Chu, A. Peters, H. Müller, Phys. Rev. Lett. 106 (2011) 151102.
[72] P. Hamilton, A. Zhmoginov, F. Robicheaux, J. Fajans, J.S. Wurtele, H. Müller, Phys. Rev. Lett. 112 (2014) 121102.
[73] S. Aghion, et al., AEgIS coll., Nat. Commun. 5 (2014) 4538.
[74] CERN-SPSC-2011-029 (http://cds.cern.ch/record/1386684/files/SPSC-P-342.pdf);
P. Pérez, et al., Hyperfine Interact. 233 (2015) 21-27;
Y. Sacquin, Eur. Phys. J. D 68 (2014) 31.
[75] P. Comini, P.A. Hervieux, F. Biraben, Hyperfine Interact. 228 (2014) 159.
[76] P. Comini, P.-A. Hervieux, New J. Phys. 15 (2013) 095022.
[77] T. Yamashita, Y. Kino, E. Hiyama, K. Piszczatowski, S. Jonsell, P. Froelich, J. Phys.: Conf. Ser. 1412 (2020) 052012.
[78] D. Ghosh, C. Sinha, Formation of antihydrogen ion in positronium-antihydrogen collision with screened Coulomb potential 2022, arXiv:2201.09225v1.
[79] S. Wolf, Ion Crystals for Fundamental Research on Matter-Antimatter Symmetry and on Photon Statistics (Ph.D. thesis), Johannes Gutenberg-Universität Mainz, 2019, https://www.quantenbit.physik.uni-mainz.de/files/2019/10/DissSW.pdf.
[80] J. Walz, T. Hänsch, Gen. Relativity Gravitation 36 (2004) 561–570.

[81] O. Rousselle, P. Cladé, S. Guellati-Khélifa, R. Guérout, S. Reynaud, Improving the statistical analysis of anti-hydrogen free fall by using near edge events 2021, arXiv:2111.06722v1;
O. Rousselle, P. Cladé, S. Guellati-Khélifa, R. Guérout, S. Reynaud, Analysis of the timing of freely falling antihydrogen 2021, arXiv:2111.02815v1.
[82] P.-P. Crépin, C. Christen, R. Guérout, V.V. Nesvizhevsky, A. Yu Voronin, S. Reynaud, Phys. Rev. A 99 (2019) 042119.
[83] C. Amole, M. Ashkezari, et al., ALPHA coll., Nat. Commun. 4 (2013) 1785.
[84] M. Ahmadi, et al., ALPHA coll., Nature 561 (2018) 211–215.
[85] G. Tino, Quantum Sci. Technol. 6 (2021) 024014.
[86] A. Yu. Voronin, P. Froelich, V.V. Nesvizhevsky, Phys. Rev. A 83 (2011) 032903.
[87] R.N. Mohapatra, G. Senjanovic, Phys. Rev. Lett. 49 (1982) 7.
[88] P. Fileviez Perez, M.B. Wise, Phys. Rev. D 84 (2011) 055015.
[89] Y. Grossman, Wee Hao Ng, S. Ray, Phys. Rev. D 98 (2018) 035020.
[90] A.A. Abdo, et al., Fermi-LAT collaboration, Astrophys. J. 703 (2009) 1249.
[91] E. Borie, M. Leon, Phys. Rev. A 21 (1980) 1460.
[92] M. Ziegler, et al., ASTERIX collaboration, Phys. Lett. 206B (1988) 151.
[93] L.M. Simons, D. Horváth, G. Torelli (Eds.), Proc. of the Fifth Course of the International School of Physics of Exotic Atoms, on Electromagnetic Cascade and Chemistry, May (1989) 14-20, Erice, Italy, Plenum Press, New York, 1990.
[94] S. Gerber, M. Doser, D. Comparat, Phys. Rev. A 100 (2019) 063418.
[95] K. Sakimoto, Eur. Phys. J. D 72 (2018) 17.
[96] L.B. Okun, Phys.-Usp. 50 (2007) 380–389.
[97] C. Vigo, L. Gerchow, B. Radics, M. Raaijmakers, A. Rubbia, P. Crivelli, Phys. Rev. Lett. 124 (2020) 101803.
[98] S. Gninenko, N.V. Krasnikov, V.A. Matveev, Phys. Rev. D 87 (2013) 015016.
[99] Z. Berezhiani, Eur. Phys. J. C 79 (2019) 484;
L.J. Broussard, et al., EPJ Web. Conf. 219 (2019) 07002;
C. Abel, et al., Phys. Lett. B 812 (2021) 135993.
[100] B. Loiseau, S. Wycech, Phys. Rev. C 102 (2020) 034006.
[101] J. Carbonell, J.M. Richard, S. Wycech, Z. Phys. A. 343 (1992) 325–329.
[102] R. Rückl, C. Zupančič, Phys. Lett. B 150 (1985) 225–229.
[103] M. Augsburger, et al., Nuclear Phys. A 658 (1999) 149–162.
[104] J. Carbonell, G. Ihle, J.M. Richard, Z. Physik A - Atomic Nuclei 334 (1989) 329–341.
[105] D. Gotta, D. Anagnostopoulos, M. Augsburger, G. Borchert, C. Castelli, D. Chatellard, et al., Nucl. Phys. A. 660 (1999) 283–321.
[106] M. Augsburger, et al., Phys. Lett. B 461 (1999) 417–422.
[107] U. Schaefer, et al., ASTERIX collaboration, Nucl. Phys. A 495 (1989) 451.
[108] C.A. Baker, et al., PS174, Nucl. Phys. A 483 (1988) 631.
[109] K. Heitlinger, et al., PS175, Z. Phys. A 342 (1992) 359.
[110] D. Gotta, in: E. Zavattini, D. Bakalov, C. Rizzi (Eds.), Frontier Tests of QED and Physics of the Vacuum, Heron Press, Sofia, 1998, pp. 170–185.
[111] J.M. Richard, M.E. Sainio, Phys. Lett. B 110 (1982) 349.
[112] G.L. Borchert, et al., Hyperfine Int. 127 (2000) 149–155.
[113] S. Wycech, A.M. Green, J.A. Niskanen, Phys. Lett. B 152 (1985) 308.
[114] R. Hayano, Nuclear Phys. A 655 (1999) 318e–323e.
[115] R. Pohl, Hyperfine Interact. 227 (2014) 23–28.
[116] M. Hori, H. Aghai-Khozani, A. Sótér, A. Dax, D. Barna, Nature 581 (2020) 37–41.
[117] M. Iwasaki, et al., Phys. Rev. Lett. 67 (1991) 1246.
[118] N. Morita, et al., Phys. Rev. Lett. 72 (1994) 1180.
[119] H. Torii, et al., Nucl. Inst. Meth. A 396 (1997) 257.
[120] V.I. Korobov, et al., Phys. Rev. Lett. 112 (2014) 103003.
[121] V.I. Korobov, et al., Phys. Rev. A 89 (2014) 032511.
[122] M.-H. Hu, et al., Chem. Phys. Lett. 654 (2016) 114.
[123] M. Hori, et al., ASACUSA collaboration, Science 354 (2016) 610.
[124] M. Hori, et al., Nature 475 (2011) 484–488.
[125] T. Pask, et al., ASACUSA collaboration, Phys. Lett. B 678 (2009) 55.
[126] S. Friedreich, et al., ASACUSA collaboration, J. Phys. B 46 (2013) 125003.
[127] R. Hughes, B. Deutsch, Phys. Rev. Lett. 69 (1992) 578.
[128] G. Gabrielse, et al., Phys. Rev. Lett. 65 (1990) 1317.
[129] P. Robertson, et al., Phys. Rev. C 16 (1977) 1945.
[130] M. Hori, Hyp. Interact. 239 (2018) 44.
[131] F. Heiße, et al., Phys. Rev. Lett. 119 (2017) 033001.
[132] S. Sturm, et al., Nature 506 (2014) 467.
[133] F. Ficek, et al., Phys. Rev. Lett. 120 (2018) 183002.
[134] V.L. Derbov, G. Chuluunbaatar, A.A. Gusev, O. Chuluunbaatar, S.I. Vinitsky, A. Góźdź, P.M. Krassovitskiy, A.V. Mitin, Proc. 11458, Saratov Fall Meeting 2019: Laser Physics, Photonic Technologies, and Molecular Modeling, Vol. 114580Q, 2020.
[135] T.P. Grozdanov, E.A. Solov'ev, Eur. Phys. J. D 74 (2020) 50.
[136] K. Richter, et al., Phys. Rev. Lett. 66 (1991) 149.
[137] S. Jonsell, P. Froelich, S. Eriksson, K. Strasburger, Phys. Rev. A 70 (2004) 062708.
[138] A. Gal, Nuclear Phys. A 699 (2002) 300–307.
[139] M. Schneider, et al., Z. Phys. A 338 (1991) 217.
[140] C.J. Batty, Nuclear Phys. A 506 (1990) 89–98.
[141] S. Wycech, A.M. Green, Z. Phys. A 344 (1992) 117.
[142] J.S. Cohen, Rep. Prog. Phys. 67 (2004) 1769.
[143] A. Bamberger, et al., Phys. Lett. B 33 (1970) 233.
[144] H. Poth, et al., Phys. Lett. B 76 (1978) 523–526.
[145] F. Hartmann, Hyperfine Interact. 119 (1999) 175.
[146] K. Sakimoto, Phys. Rev. A 74 (2006) 022709.
[147] K.B. MacAdam, L.G. Gray, R.G. Rolfes, Phys. Rev. A 42 (1990) 5269.
[148] P. Yzombard, M. Hamamda, S. Gerber, M. Doser, D.I. Comparat, Phys. Rev. Lett. 114 (2015) 213001.
[149] D. Gotta, K. Rashid, B. Fricke, P. Indelicato, L.M. Simons, Eur. Phys. J. D 47 (2008) 11.

[150] M.R. Flannery, D. Vrinceanu, Int. J. Mass Spectr. 223–224 (2003) 473–489.
[151] X. Sun, K.B. MacAdam, Phys. Rev. A 47 (1993) 3913.
[152] T.P. Grozdanov, R.K. Janev, L.P. Presnyakov, D.B. Uskov, Phys. Lett. A 109 (1985) 93.
[153] J.E. Russell, Phys. Rev. A 1 (1970) 721;
J.E. Russell, Phys. Rev. A 1 (1970) 735;
J.E. Russell, Phys. Rev. A 1 (1970) 742.
[154] R. Ahlrichs, et al., Z. Phys. A - Atoms Nuclei 306 (1982) 297–300.
[155] J. Révai, V.B. Belyaev, Phys. Rev. A 67 (2003) 032507.
[156] K. Sakimoto, Phys. Rev. A 84 (2011) 032501.
[157] E. Widmann, et al., Phys. Rev. A 51 (1995) 2870.
[158] M. Hori, V. Korobov, Phys. Rev. A 81 (2010) 062508.
[159] P. Brax, C. van de Bruck, A.-C. Davis, Phys. Rev. Lett. 99 (2007) 121103.
[160] R. Foot, X.-G. He, Phys. Lett. B 267 (1991) 509.
[161] M. Jones, R. Potvliege, M. Spannowsky, Phys. Rev. Res. 2 (2020) 013244.
[162] R. Bacher, P. Blüm, D. Gotta, K. Heitlinger, M. Schneider, J. Missimer, L.M. Simons, K. Elsener, Phys. Rev. A 38 (1988) 4395.
[163] E. Taralli, et al., IEEE Trans. Appl. Superconduct. 31 (2021) 2100605, http://dx.doi.org/10.1109/TASC.2021.3061022, 1-5.
[164] D. Grzonka, et al., Hyperfine Interact. 240 (2019) 22.
[165] E. Steffens, AIP Conf. Proc. 1149 (2009) 80–89.
[166] H.O. Meyer, AIP Conf. Proc. 1008 (2008) 124–131.
[167] B. Schoch, Eur. Phys. J. A 43 (2010) 5–9.
[168] P. Lenisa, F. Rathmann, for the PAX collaboration, Antiproton–proton scattering experiments with polarization 2005, arXiv:hep-ex/0505054v1.
[169] K. Imai, AIP Conf. Proc. 145 (1986) 229.
[170] Th Wörmann, Z. Roller-Lutz, H.O. Lutz, Phys. Rev. A 47 (1993) R1594(R).
[171] A. Kastler, J. Phys. Radium 11 (1950) 255–265, http://dx.doi.org/10.1051/jphysrad:01950001106025500.
[172] Hongying Yang, Yanhua Wang, Nan Zhao, Eur. Phys. J. D 74 (2020) 225.
[173] T.P. Rakitzis, et al., Science 300 (5627) (2003) 1936–1938.
[174] V. Anastassopoulos, et al., Rev. Sci. Instrum. 87 (2016) 115116.
[175] J.P. Desclaux, in: E. Clementi (Ed.), Methods and Techniques in Computational Chemistry, Vol. A: Small Systems of METTEC, STEF, Cagliari, 1993, p. 253, P. Indelicato and J.P. Desclaux, MCDFGME, A Multiconfiguration Dirack-Fock and General Matrix Elements Program (release 2005) http://dirac.spectro.jussieu.fr/mcdf.
[176] J.-H. Choi, J.R. Guest, A.P. Povilus, E. Hansis, G. Raithel, Phys. Rev. Lett. 95 (2005) 243001.
[177] T. Pohl, H.R. Sadeghpour, P. Schmelcher, Phys. Rep. 484 (2009) 181–229.
[178] D. Comparat, C. Malbrunot, Phys. Rev. A 99 (2019) 013418; Erratum Phys. Rev. A 101 (2020) 019904.
[179] C.J. Batty, E. Friedman, A. Gal, Nuclear Phys. A 689 (2001) 721–740.
[180] E. Friedman, A. Gal, B. Loiseau, S. Wycech, Nuclear Phys. A 943 (2015) 101.
[181] Teck-Ghee Lee, Cheuk-Yin Wong, Phys. Rev. C 97 (2018) 054617.
[182] W. Kanert, et al., Phys. Rev. Lett. 56 (1986) 2368.
[183] W. Kanert, et al., Z. Phys. A 326 (1987) 523.
[184] S. Wycech, et al., Nuclear Phys. A 561 (1993) 607–627.
[185] H. Poth, et al., Nuclear Phys. A 294 (1978) 435–449.
[186] R. Guigas, P. Blüm, H. Koch, M. Meyer, Phys. Lett. B 137 (1984) 323–328.
[187] A. Kreissl, et al., Z. Phys. A 329 (1988) 235–241.
[188] A. Trzcinska, PS209 collaboration, Phys. Rev. Lett. 87 (2001) 082501.
[189] P. Lubiński, et al., Phys. Rev. C 57 (1998) 2962.
[190] R. Schmidt, et al., Phys. Rev. C 60 (1999) 054309.
[191] P. Lubiński, (Ph.D. thesis), Warsaw University, 1997, unpublished.
[192] B. Klos, et al., Phys. Rev. C 76 (2007) 014311.
[193] S. Wycech, F. Hartmann, J. Jastrzebski, B. Klos, A. Trzcinska, T. von Egidy, Phys. Rev. C 76 (2007) 014311.
[194] M. Centelles, X. Roca-Maza, X. Viñas, M. Warda, Phys. Rev. Lett. 102 (2009) 122502;
M. Warda, X. Viñas, X. Roca-Maza, M. Centelles, Phys. Rev. C 80 (2009) 024316.
[195] M.B. Tsang, et al., Phys. Rev. C 86 (2012) 015803.
[196] S. Abrahamyan, et al., PREX collaboration, Phys. Rev. Lett. 108 (2012) 112502.
[197] A. Kreissl, et al., Z. Phys. C 37 (1988) 557–561.
[198] F. Balestra, et al., Nuclear Phys. A 465 (1987) 714.
[199] F. Balestra, et al., Nuclear Phys. A 491 (1989) 541.
[200] M. Warda, X. Viñas, X. Roca-Qaza, M. Centelles, Phys. Rev. C 80 (2009) 024316.
[201] M. Thiel, et al., J. Phys. G: Nucl. Part. Phys. 46 (2019) 093003.
[202] J. Hratankova, J. Mares, Nuclear Phys. A 969 (2018) 45–49.
[203] J. Hratankova, J. Mares, Nuclear Phys. A 945 (2016) 197–215.
[204] Xian-Wei Kang, J. Haidenbauer, Ulf-G. Meißner, Phys. Rev. D 91 (2015) 074003.
[205] J. Haidenbauer, C. Hanhart, Xian-Wei Kang, Ulf-G. Meißner, Phys. Rev. D 92 (2015) 054032.
[206] P. Jasselette, J. Cugnon, J. Vandermeulen, Nuclear Phys. A 484 (1988) 542.
[207] Zhao-Qing Feng, Phys. Rev. C 94 (2016) 064601.
[208] P. Lubinski, A. Grochulska, T. von Egidy, J. Gulda, F.J. Hartmann, J. Jastrzebski, W. Kurcewicz, L. Pienkowski, A. Stolarz, A. Trzcinska, Phys. Rev. C 66 (2002) 044616.
[209] E.F. Moser, H. Daniel, T. von Egidy, et al., Z. Phys. A 333 (1989) 89–105.
[210] T. von Egidy, Nature 328 (1987) 773–778.
[211] W. Markiel, et al., Nuclear Phys. A 485 (1988) 445–460.
[212] E.F. Moser, et al., Phys. Lett. B 179 (1986) 25.
[213] G. Cerchiari, et al., in preparation.
[214] Zhao-Qing Feng, Phys. Rev. C 93 (2016) 041601.
[215] A.B. Larionov, T. Gaitanos, U. Mosel, Hyperfine Interact. 213 (1-2) (2012) 81–87.
[216] M. Agnello, et al., Nucl. Instrum. Methods Phys. Res. A 399 (1997) 11–26.
[217] K.V. Protasov, V. Gudkov, E.A. Kupriyanova, V.V. Nesvizhevsky, W.M. Snow, A. Yu Voronin, Phys. Rev. D 102 (2020) 075025.
[218] A. Bracco, F. Camera, F.C.L. Crespi, et al., Eur. Phys. J. A 55 (2019) 233.

[219] D.F. Measday, Phys. Rep. 354 (2001) 243.
[220] A. Knecht, A. Skawran, S. Vogiatzi, Eur. Phys. J. Plus 135 (2020) 777.
[221] A. Antognini, et al., Phys. Rev. C 101 (2020) 054313.
[222] E.V. Tkalya, Phys. Rev. A 94 (2016) 012510.
[223] S. Schmidt, et al., J. Phys.: Conf. Ser. 1138 (2018) 012010.
[224] G. Bollen, et al., Phys. Rev. C 46 (1992) R2140(R).
[225] S. Ayet San Andrés, et al., Phys. Rev. C 99 (2019) 064313.
[226] D. Vrinceanu, S.X. Hu, S. Mazavet, L.A. Collins, Phys. Rev. A 72 (2005) 042503.
[227] C.A. Yazeljian, J.C. Straton, Eur. Phys. J. D 74 (2020) 156.
[228] A. Jacob, et al., Phys. Rev. Res. 2 (2020) 013105.
[229] L. Hilico, et al., Int. J. Mod. Phys. Conf. Ser. 30 (2014) 1460269, http://dx.doi.org/10.1142/S2010194514602695.
[230] A.R. Swann, D.B. Cassidy, A. Deller, G.F. Gribakin, Phys. Rev. A 93 (2016) 052712.
[231] T. Yamashita, et al., New J. Phys. 23 (2021) 012001.
[232] E.A.G. Armour, J.-M. Richard, K. Varga, Phys. Rep. Vol. 413 (2005) 1–90.
[233] J. Mitroy, J. Phys. B: At. Mol. Opt. Phys. 33 (2000) 5307.
[234] M. Abdel-Raouf, J. Phys. : Conf. Ser. 194 (2009) 072003.
[235] B.D. Esry, H.R. Sadeghpour, Phys. Rev. A 67 (2003) 012704.
[236] S. Chandrasekar, Agron. J. 100 (1944) 176.
[237] M. Genkin, E. Lindroth, Eur. Phys. J. D 51 (2009) 205.
[238] P. Indelicato, J. Phys. B: At. Mol. Opt. Phys. 52 (2019) 23.
[239] Hannspeter Winter, Friedrich Aumayr, J. Phys. B: At. Mol. Opt. Phys. 32 (1999) R39.
[240] U.D. Jentschura, P.J. Mohr, J.N. Tan, J. Phys. B: At. Mol. Opt. Phys. 43 (2010) 074002.
[241] D. Bressanini, M. Mella, G. Morosi, Phys. Rev. A 55 (1997) 200.
[242] B.L. Hammond, W.A. Lester Jr., P.J. Reynolds, Monte Carlo Methods in Ab Initio Quantum Chemistry, first ed., World Scientific, Singapore, 1994.
[243] V. Bendkowsky, B. Butscher, J. Nipper, J.P. Shaffer, R. Löw, T. Pfau, Nature 458 (2009) 1005–1008.
[244] Y.K. Ho, Phys. Rev. A 39 (1989) 2709.
[245] F. Lang, K. Winkler, C. Strauss, R. Grimm, J.H. Denschlag, Phys. Rev. Lett. 101 (2008) 133005.
[246] J. Deiglmayr, A. Grochola, M. Repp, K. Mörtlbauer, C. Glück, J. Lange, O. Dulieu, R. Wester, M. WeidemM̈ller, Phys. Rev. Lett. 101 (2008) 133004.
[247] A. Schenck, et al., in: Jungmann K.P., Kowalski J., Reinhard I., Träger F. (Eds.), Atomic Physics Methods in Modern Research, in: Lecture Notes in Physics, vol. 499, Springer, Berlin, Heidelberg, http://dx.doi.org/10.1007/BFb0104336.
[248] M. Saunders, et al., Science 271 (5256) (1996) 1693–1697.
[249] S. Aoyagi, et al., Nature Chem. 2 (2010) 678–683.
[250] C. Foroutan-Neja, M. Straka, I. Fernandéz, G. Frenking, Ang. Chemie 57 (42) (2018) 13931–13934.
[251] J-Ph Karr, J. Mol. Spectr. 300 (2014) 37–43.
[252] E.G. Myers, Phys. Rev. A 98 (2018) 010101(R).
[253] E.G. Myers, Hyperfine Interact. 239 (2018) 43.
[254] M. Emami-Razavi, J. Darewych, Eur. Phys. J. D 75 (2021) 188.
[255] M. Cheret, et al., J. Phys. B: At. Mol. Phys. 15 (1982) 3463.
[256] D. Sardar, S. Naskar, A. Pal, H. Berriche, B. Deb, J. Phys. B: At. Mol. Opt. Phys. 49 (2016) 245202.
[257] M. Beyer, F. Merkt, Phys. Rev. X 8 (2018) 031085.
[258] M. Zammit, et al., Phys. Rev. A 100 (2019) 042709.
[259] E.G. Myers, L. Hilico, J.P. Karr, Beyond Antihydrogen: testing CPT with the Antihydrogen Molecular Ion, CERN-SPSC-2019-034, https://cds.cern.ch/record/2691253/files/SPSC-M-790.pdf.
[260] A. Petrignani, et al., J. Chem. Phys. 141 (2014) 241104.
[261] C.R. Markus, B.J. McCall, J. Chem. Phys. 150 (2019) 214303.
[262] Jon T. Hougen, J. Chem. Phys. 37 (1962) 1433.
[263] E. Armour, W. Byers Brown, Acc. Chem. Res. 26 (1993) 168–173.
[264] A. Frolov, J. Phys. B: AAt. Mol. Opt. Phys. 46 (2013) 125001.
[265] F. Schmidt-Kaler, et al., New J. Phys. 13 (2011) 075014.
[266] T. Feldker, P. Bachor, M. Stappel, D. Kolbe, R. Gerritsma, J. Walz, F. Schmidt-Kaler, Phys. Rev. Lett. 115 (2015) 173001.
[267] P. Bachor, et al., J. Phys. B: At. Mol. Opt. Phys. 49 (2016) 154004.
[268] C. Zhang, F. Pokorny, W. Li, et al., Nature 580 (2020) 345–349.
[269] M. Deiß, S. Haze, J. Hecker Denschlag, Atoms 9 (2021) 34, http://dx.doi.org/10.3390/atoms9020034.
[270] A. Duspayev, X. Han, M.A. Viray, L. Ma, J. Zhao, G. Raithel, Phys. Rev. Res. 3 (2021) 023114.
[271] H. da Silva, M. Raoult, M. Aymar, O. Dulieu, New J. Phys. 17 (2015) 045015.
[272] Kenneth D. Jordan, Feng Wang, Ann. Rev. Phys. Chem. 54 (1) (2003) 367–396.
[273] T.J. Millar, C. Walsh, T.A. Field, Chem. Rev. 117 (3) (2017) 1765–1795.
[274] M.C. McCarthy, C.A. Gottlieb, H. Gupta, P. Thaddeus, Agron. J. 652 (2006) L141.
[275] Victor G. Bezchastnov, Peter Schmelcher, Lorenz S. Cederbaum, Phys. Rev. A 75 (2007) 052507.
[276] C. Fey, F. Hummel, P. Schmelcher, Mol. Phys. 118 (2) (2020) e1679401.
[277] F. Engel, et al., Phys. Rev. Lett. 123 (2019) 073003.